Rb Regulates DNA Damage Response and Cellular Senescence through E2F-dependent Suppression of N-Ras Isoprenylation

Awad Shamma,[1,2] Yujiro Takegami,[1] Takao Miki,[1,2] Shunsuke Kitajima[1], Makoto Noda[1], Takao Obara,[3] Takahiro Okamoto,[3]

and Chiaki Takahashi [1,2,*]

[1] Department of Molecular Oncology, Kyoto University Graduate School of Medicine, Kyoto 606-8501, Japan

[2] The 21st Century Center of Excellence Formation, Kyoto University Graduate School of Medicine, Kyoto 606-8501, Japan

[3] Department of Endocrine Surgery, Tokyo Women's Medical University, Tokyo 166-8666, Japan

[*] Correspondence: chtakaha@virus.kyoto-u.ac.jp

TEL: +81-75-751-4151

FAX: +81-75-751-4159

Running title: Rb regulates Ras isoprenylation

Summary

Oncogene-induced cellular senescence (OIS) is well documented, but little is known about how infinite cell proliferation induced by loss of tumor suppressor genes is antagonized by cellular functions. *Rb* heterozygous mice generate *Rb*-deificient C-cell adenomas that progress to adenocarcinomas following bialelic loss of *N-ras*. Here, we demonstrate that pRb inactivation induces abberant expression of *farnesyl dipshosphate synthase*, many of *prenyltransferases* and their upstream regulators *sterol regulatory element binding proteins* (*SREBPs*) in an E2F-dependent manner, leading to enhanced isoprenylation and activation of N-Ras. Consequently, elevated N-Ras activity induces DNA damage response (DDR) and p130-dependent cellular senescence in *Rb*-deficient cells. Futhermore, *Rb* heterozygous mice additionally lacking any of *Ink4a*, *Arf* or *Suv39h1* generated C-cell adenocarcinomas, suggesting that cellular senescence antagonizes *Rb*-deficient carcinogenesis.

SIGNIFICANCE

Aberration of the pRB pathway critically pertains to human carcinogenesis. However, germ line *RB* mutations are detected in a limited variety of malignant tumors, implicating the presence of defense mechanisms antagonizing *RB*-deficient tumorigenesis. In this study, we attempted to clarify the mechanism by which *N-ras* loci protect mouse C-cells and primary fibroblasts from *Rb*-loss-induced carcinogenesis, and revealed a function of pRb in regulating post-

translational modification of CAAX proteins. Our findings explain the tumor suppressor function of N-Ras in certain types of cells lacking pRb. In addition, since Ras proteins promote carcinogenesis in many cell types, our findings may provide rational basis for the application of prenyltransferase inhibitors to human cancers with aberrations in the pRB pathway.

Introduction

Carcinogenesis is induced by the breakdown of cellular functions that counteract various oncogenic stimuli (Hanahan and Weinberg, 2000). OIS was first noted as paradoxical growth arrest in human diploid fibroblasts induced by oncogenic Ras (Collado et al., 2007). Currently, OIS is accepted as the cellular function that antagonizes carcinogenesis, despite the presence of oncogenic mutation. The study of melanocytic nevi carrying the $BRAF^{V600E}$ mutation provided the first evidence of cellular senescence in human premalignant lesions (Mooi and Peeper, 2006). Thereafter, the number of OIS inducers identified has been rapidly increasing (Di Micco et al., 2007).

OIS is achieved by activating tumor suppressors including $p16^{INK4a}$, ARF, pRB and p53, or by inducing DDR activation engaged by γH2AX, Chk2, p53 and ATM before critical telomeric attrition occurs (Collado et al., 2007; Di Micco et al., 2007). These cellular functions counteract infinite cell proliferation induced by oncogenic signals. Accelerated cell proliferation induced by the loss of tumor

suppressors can be counteracted by similar functions. For example, *PTEN*-loss-induced prostate carcinogenesis is antagonized by p53-mediated senescence (Chen et al., 2005), and *VHL* loss-induced cellular senescence is mediated by pRB and p400 (Young et al., 2008). In human retinoblastoma, additional aberration in p53 pathway is required for carcinogenesis (Laurie et al., 2006). Nevertheless, we suspect that *RB*-deficiency in the human body can be antagonized in many ways, because of the diversified functions of pRB and the limited variety of mouse and human cell types that develop tumor with germ line *RB* mutations (Wikenheiser-Brokamp, 2006).

$Rb^{+/-}$ mice generate C-cell adenoma in the thyroid following somatic loss of the normal *Rb* allele. Additional loss of *N-ras* alleles induces malignant conversion in *Rb*-deficient C-cell adenoma. Moreover, somatic *N-ras* loss frequently occurs in $Rb^{+/-}$;$N\text{-}ras^{+/-}$ C-cells following *Rb*-loss, causing spontaneous malignant conversion (Takahashi et al., 2006). The C-cell tumor phenotype observed in $Rb^{+/-}$;$E2F3^{-/-}$ mice (Ziebold et al., 2003) is similar to that in $Rb^{+/-}$;$N\text{-}ras^{-/-}$ mice. It was proposed that the Rb-E2F complex functions as a transcriptional repressor to antagonize Ras signaling during vulval formation in *Caenorhabditis.elegans* (Ceol and Horvitz, 2001). The *Rb-ras* genetic interaction during cell differentiation, embryogenesis and tumorigenesis has been extensively investigated in mice (Lee et al., 1999; Takahashi et al., 2003; Takahashi et al., 2004; Takahashi et al., 2006), however, the core mechanism of this interaction

has not yet been clarified. In this study, we seeked *in vitro* and *in vivo* evidence that *Rb*-loss-induced cell proliferation in mouse C-cells and primary fibroblasts is counteracted by an N-Ras-dependent senescence pathway, and attempted to elucidate the mechanism by which pRb regulates N-Ras activation.

Results

N-ras-dependent DDR and cellular senescence in *Rb*-deficient C-cell adenoma

To investigate how N-Ras prevents *Rb*-deficient C-cell adenoma from progressing to adenocarcinoma (Figure 1A), we analyzed primary C-cell tumors developed in $Rb^{+/-}$;$N\text{-}ras^{+/+}$ (average age at examination (AE) ± standard error (SE) = 11.0 ± 1.2 months) and $Rb^{+/-}$;$N\text{-}ras^{-/-}$ (AE = 10.6 ± 0.9) mice. Proliferating cell nuclear antigen (PCNA) and Ki-67 were frequently expressed in *Rb*-deficient $N\text{-}ras^{-/-}$ adenocarcinomas, but their expression was invariably rare in *Rb*-deficient $N\text{-}ras^{+/+}$ adenomas (Figure 1B). On the other hand, *Rb*-deficient $N\text{-}ras^{+/+}$ adenomas frequently expressed DDR markers (Shiloh, 2003) including H2AX phosphorylated at serine 139 (γH2AX), ATM phosphorylated at serine 1981 (ATMpS1981) and p53 phosphorylated at serine 15 (p53pS15). These markers were rarely detected in $N\text{-}ras^{-/-}$ adenocarcinomas (Figure 1B). In addition, $N\text{-}ras^{+/+}$ tumors frequently expressed senescence markers (Dimri, 2005) including histone H3 tri-methylated at serine 9 (H3K9me3), heterochromatin protein 1γ (HP1γ), $p16^{Ink4a}$ and senescence-associated-β-

galactosidase (SA-β-gal) activity. These markers were rarely detected in *N-ras*$^{-/-}$ adenocarcinomas (Figure 1B) or in adenocarcinomas spontaneously developed in *Rb*$^{+/-}$;*N-ras*$^{+/-}$ mice as a consequence of somatic loss of *N-ras* allele following *Rb*-loss (Figure S1). These findings suggest that *N-ras* loci induce DDR and cellular senescence during adenoma formation initiated by *Rb*-loss. We therefore hypothesized that N-Ras prevents *Rb*-deficient C-cell adenomas from progressing to adenocarcinomas by inducing DDR and cellular senescence.

To determine the sequence of events during development of an adenoma, we compared *Rb*-deficient adenomas developed in younger *Rb*$^{+/-}$ mice (early adenoma; AE = 6.2 ± 0.3) to those in older mice (late adenoma; AE = 11.0 ± 1.2). DDR markers were expressed in early and late adenomas with similar frequencies, however, senescence markers were less frequently expressed in early adenomas (Figure S2). In contrast, PCNA and Ki-67 were more frequently expressed in early adenomas than in late adenomas. These findings suggest that DDR may precede cellular senescence during the development of C-cell adenoma initiated by *Rb*-loss, and that early adenomas grow even in the presence of DDR, but cease to grow when cellular senescence is induced.

Role of senescence-mediating genes in *Rb*-deficient C-cell adenoma

To examine whether cellular senescence protects *Rb*-deficient C-cell adenomas from progressing to adenocarcinoma, we generated *Rb*$^{+/-}$ mice simultaneously

lacking *Ink4a*, *Ink4a* and *Arf*, *Arf* or *Suv39h1*. All $Rb^{+/-}$;$Ink4a^{-/-}$ mice survived longer than 8 months (n = 12). The average age at the onset of sickness or death (SD) was 9.3 ± 0.4 months in $Rb^{+/-}$;$Ink4a^{+/+}$ (n = 7), 9.5 ± 0.6 in $Rb^{+/-}$;$Ink4a^{+/-}$ (n = 3), and 9.7 ± 0.4 in $Rb^{+/-}$;$Ink4a^{-/-}$ (n = 6) mice. No acceleration of *Rb*-deficient pituitary tumorigenesis was observed in the $Ink4a^{-/-}$ background (data not shown). All $Rb^{+/-}$;$Ink4a^{-/-}$ mice exhibited large macroscopic tumors stemming from the thyroid (Figure 2A and Table 1). $Rb^{+/-}$;$Ink4a^{+/-}$ mice generated macroscopic tumors, but these were smaller than those in $Rb^{+/-}$;$Ink4a^{-/-}$ mice. No macroscopic thyroid tumors were observed in $Rb^{+/-}$;$Ink4a^{+/+}$ mice. Histologically, all thyroid tumors developed in $Rb^{+/-}$;$Ink4a^{-/-}$ and $Rb^{+/-}$;$Ink4a^{+/-}$ mice exhibited features of C-cell adenocarcinoma (Figure 2B and Table 1) and were histologically similar to tumors developed in $Rb^{+/-}$;$N\text{-}ras^{-/-}$ mice. $Rb^{+/+}$;$Ink4a^{-/-}$ mice showed no evidence of microscopic thyroid tumor. *Rb*-deficient $Ink4a^{-/-}$ cells separated from primary tumors grew in tissue culture and expressed calcitonin (5 successful cultures from 6 attempts with independent tumors) (Figure 2C), as did *Rb*-deficient $N\text{-}ras^{-/-}$ C-cell adenocarcinoma cells. However, no clonally expanding calcitonin-positive cells were derived from thyroids harboring *Rb*-deficient $Ink4a^{+/+}$ tumors (0/6), suggesting that, as did *Rb*-deficient $N\text{-}ras^{-/-}$ C-cells, *Rb*-deficient $Ink4a^{-/-}$ C-cell tumor cells had acquired the ability to infinitely proliferate. Therefore, we diagnosed tumors developed in $Rb^{+/-}$;$Ink4a^{-/-}$ mice as C-cell adenocarcinomas. These findings suggest that C-cell carcinogenesis initiated by *Rb*-loss is blocked by *Ink4a*.

Rb$^{+/-}$;*Ink4a*$^{-/-}$;*Arf*$^{-/-}$ (SD = 5.3 ± 0.1; n = 9) and *Rb*$^{+/-}$;*Arf*$^{-/-}$ (SD = 4.7 ± 0.2; n = 3) mice died of lymphoma, sarcoma or, more often, of accelerated pituitary tumor growth as described previously (Tsai et al., 2002), before they developed macroscopic thyroid tumors. However, at 4.8 months, *Rb*$^{+/-}$;*Ink4a*$^{-/-}$;*Arf*$^{-/-}$ mice developed large microscopic adenocarcinomas with a morphology different from that of *Rb*-deficient *N-ras*$^{-/-}$ or *Rb*-deficient *Ink4a*$^{-/-}$ tumors (Figure 2B). *Rb*$^{+/+}$;*Ink4a*$^{-/-}$;*Arf*$^{-/-}$ mice of the same age or older showed no evidence of microscopic thyroid tumor (Table 1). In *Rb*$^{+/-}$;*Arf*$^{-/-}$ mice (AE = 5.2 ± 0.3) but not in *Rb*$^{+/+}$;*Arf*$^{-/-}$ mice, we often observed large microscopic adenocarcinomas with morphologies different from those in *Rb*-deficient *N-ras*$^{-/-}$, *Rb*-deficient *Ink4a*$^{-/-}$ or *Rb*-deficient *Ink4a*$^{-/-}$;*Arf*$^{-/-}$ tumors. Tumor cells separated from *Rb*$^{+/-}$;*Ink4a*$^{-/-}$;*Arf*$^{-/-}$ (3/3) and *Rb*$^{+/-}$;*Arf*$^{-/-}$ (2/2) mice grew in tissue culture and expressed calcitonin. However, in an *Arf*$^{-/-}$ background, regardless of the *Ink4a* genotype, and despite the frequent PCNA and Ki-67 expression and infinite growth in culture, the frequency of carcinoembryonic antigen (CEA)-positive C-cell tumor cells was low (Figure 2B and Table 1). This suggests a specific genetic interaction between *Arf* and *CEA*. *Rb*$^{+/-}$;*Suv39h1*$^{-/-}$ mice (AE = 4.6 ± 0.2) exhibited macroscopic tumors (Figure 2A and Table 1) that grew in tissue culture (2/2) (Figure 2C), and frequently expressed CEA, PCNA and Ki-67 (Figure 2B and Table 1). These findings suggest that *p16*^{Ink4a}, *Arf* and *Suv39h1* antagonize *Rb*-deficient C-cell carcinogenesis.

Role of N-Ras in *Rb*-deficient C-cell carcinogenesis

We generated 11 cell lines from independent primary *Rb*-deficient *N-ras*$^{-/-}$ thyroid tumors, all of them were calcitonin positive (data not shown). Six cell lines were less adhesive. Five adhesive cell lines were competent for transfection and infection. After transduction of N-Ras or N-Ras^{V12}, all of the adhesive cell lines grew without immediate growth arrest or cell death for a minimum of 5 days. Moreover, upon subcutaneous inoculation into nude mice, one of the adhesive cell lines, AC61, produced tumors histologically similar to primary *Rb*-deficient *N-ras*$^{-/-}$ tumors. Importantly, this cell line generated smaller subcutaneous tumors with features of *Rb*-deficient adenomas when reconstituted with N-Ras at a level comparable to that of endogenous N-Ras expressed in an *Rb*-positive and *ret* mutation-positive human C-cell adenocarcinoma cell line TT (Tomoda et al., 2008) (Figure 3A).

Nine days after *N-ras* transduction, we observed a marked induction of DDR (Figure 3B). Comet assay detected a high frequency DNA double strand breaks in N-Ras-transduced cells within 10 days (Figure 3C). At day 14, senescence markers including Suv39h1, H3K9me3 and HP1γ recruited to the chromatin, p16^{Ink4a}, p19^{Arf} and nuclear p130 were readily detectable (Figure 3D and E). We also detected senescence-associated heterochromatin foci (SAHF) (Narita et al., 2003) (Figure 3D) and high SA-β-gal activity (Figure 3F). The other 4 cell lines

(AC55, 62, 65 and 69) responded to N-Ras in a manner similar to AC61 (Figure S3). We did not detect telomerase (mTERT) expression in AC61 cells. The AC55 cell line was telomerase-positive. However, N-Ras transduction did not significantly change mTERT expression nor telomerase activity in AC55 cells, excluding the possibility of replicative senescence (Figure S4A-C). These findings indicate that in the absence of pRb, N-Ras induces DNA damage and cellular senescence that functions as a barrier against C-cell carcinogenesis.

p130-dependent differential functions of wild-type and oncogenic N-Ras in the absence of pRb

When introduced into AC61 cells, N-Ras^{V12} was far less efficient at inducing DDR and senescence markers (Figure 3B-E), growth arrest and SA-β-gal activity (Figure 3F), compared to N-Ras. Further, we observed only a slight decrease in the proliferation of pRb-reconstituted AC61 cells suggesting that AC61 cells were reprogrammed to be no more addicted to *Rb*-loss (Figure 3F). The effects of N-Ras and N-Ras^{V12} in inducing cellular senescence were reversed after pRb reconstitution (Figure 3F). These findings suggest that pRb attenuates N-Ras function to induce cellular senescence in AC61 cells and that N-Ras^{V12} fails to activate alternative cellular senescence programs when pRb is unavailable.

We observed that p130 was markedly induced and accumulated in the nuclei of

AC61 cells transduced with N-Ras, but not in AC61 cells transduced with N-Ras^{V12} (Figure 3E and G). Nuclear p130 was complexed with Suv39h1, H3K9me3 and HP1γ in the presence of N-Ras, but not N-Ras^{V12} (Figure 3G). In consistent, we detected the colocalization of p130 and HP1γ signals in the nuclei of N-Ras-reconstituted cells (Figure 3G). N-Ras failed to induce cellular senescence in AC61 cells when p130 was depleted beforehand by specific shRNAs (Figure 3H and S5A). Moreover, p130 depletion at day 14 after N-Ras transduction, significantly reversed cellular senescence (Figure 3I and S5B). These findings suggest that p130 is required for induction and maintenance of N-Ras-induced cellular senescence in *Rb*-deficient cells. We also observed significant p130 induction in primary C-cell adenomas developed in *Rb*$^{+/-}$;*N-ras*$^{+/+}$ mice, but not in adenocarcinomas developed in *Rb*$^{+/-}$;*N-ras*$^{-/-}$ mice (Figure 3J). Taken together, these findings suggest that induction of p130 is critical for cellular senescence induced by N-Ras in *Rb*-deficient C-cell adenocarcinoma cells, and that N-Ras^{V12} fails to induce cellular senescence in these cells due to inability to induce p130.

Rb$^{-/-}$;*N-ras*$^{-/-}$ MEFs escape cellular senescence

To generalize our observation on C-cells, we characterized mouse embryo fibroblasts (MEFs) prepared from *Rb*$^{-/-}$ embryos with various *N-ras* genotypes. During the serial passages according to the 3T3 protocol (Todaro and Green, 1963), *Rb*$^{-/-}$;*N-ras*$^{-/-}$ MEFs achieved infinite proliferation significantly earlier than

Rb$^{-/-}$ MEFs (Figure 4A). *Rb*$^{-/-}$;*Ink4a*$^{-/-}$ MEFs exhibited proliferative characteristics similar to those of *Rb*$^{-/-}$;*N-ras*$^{-/-}$ MEFs.

Rb$^{-/-}$;*N-ras*$^{-/-}$ MEFs but not *Rb*$^{+/+}$;*N-ras*$^{+/+}$, *Rb*$^{-/-}$;*N-ras*$^{+/+}$ or *Rb*$^{+/+}$;*N-ras*$^{-/-}$ MEFs, could form colonies when plated at low cell density (Figure 4B). Moreover, shRNA-directed N-Ras depletion in *Rb*$^{-/-}$ MEFs allowed them to form colonies under the same conditions (Figure 4C). Further, *Rb*$^{-/-}$;*Ink4a*$^{-/-}$ MEFs formed colonies when plated at low cell density, which was suppressed by p16^{INK4a}. Colony formation by *Rb*$^{-/-}$;*N-ras*$^{-/-}$ MEFs was suppressed by N-Ras, pRb or p16^{INK4a}, but not by N-Ras^{V12} (Figure 4D). N-Ras^{N17} did not reduce colony numbers, albeit at smaller colony size, suggesting that the function of N-Ras in colony suppression depends on GTP. The colony suppression in *Rb*$^{-/-}$;*N-ras*$^{-/-}$ MEFs induced by N-Ras was due to cellular senescence (Figure 4E and S6). N-Ras^{V12} and other activated Ras isoforms did not induce cellular senescence but induced transformation in *Rb*$^{-/-}$;*N-ras*$^{-/-}$ MEFs (Figure 4E and F). However, *Rb*$^{+/+}$;*N-ras*$^{-/-}$ MEFs (Figure 4E) and wild-type MEFs (data not shown) were senesced by N-Ras^{V12}. A previous study demonstrated that *Rb*$^{-/-}$;*p107*$^{-/-}$;*p130*$^{-/-}$ MEFs escaped cellular senescence and were efficiently transformed by H-Ras^{V12} (Sage et al., 2000). Similarly, *Rb*$^{-/-}$;*N-ras*$^{-/-}$ MEFs were transformed by all isoforms of Ras^{V12} (Figure 4F). These findings suggest that MEFs can be transformed by Ras^{V12} once exempted from senescence program, and thereby support the hypothesis that *Rb*$^{-/-}$;*N-ras*$^{-/-}$ MEFs escaped cellular senescence.

Finally, to further elucidate the differential functions of N-Ras and N-Ras^{V12} in the absence of pRb, both proteins were simultaneously expressed in *Rb*$^{-/-}$;*N-ras*$^{-/-}$ MEFs. N-Ras was dominant over N-Ras^{V12} in inducing DDR and most of the senescence markers, but N-Ras^{V12} antagonized N-Ras activity to induce p16^{Ink4a} in the absence of *Rb* (Figure S6). These findings suggest that N-Ras and N-Ras^{V12} exert many different biological functions in the absence of *Rb*. To explain this difference, we analyzed the activation mechanisms of them in the studies discussed below.

pRb attenuates N-Ras activity in C-cell adenocarcinoma

To address why N-Ras and N-Ras^{V12} exert different functions in the absence of pRb, we again analyzed AC61 cells. N-Ras expressed in AC61 cells was significantly activated, however, the activity was decreased to 10.4% (9.6 to 1.0) when pRb was simultaneously expressed under the influence of a strong promoter (Figure 5A). The relative activation level of N-Ras^{V12} (65.1) was 6.8 times higher than that of N-Ras (9.6) in the absence of pRb. The activity of N-Ras^{V12} was also attenuated by pRb, but this attenuation was less efficient (65.1 to 37.5) than that of N-Ras (9.6 to 1.0). Freshly introduced exogenous pRb was hyperphosphorylated when coexpressed with N-Ras^{V12} compared to N-Ras (Figure 5A) as previously shown (Peeper et al., 1997). We therefore considered that hypophosphorylated pRb is more potent than hyperphosphorylated pRb in

suppressing N-Ras activity. These findings suggest that in the absence of pRb, the activation level of N-Ras is moderate yet significantly lower than that of N-Ras^{V12}. This may at least partially explain the differential functions of N-Ras and N-Ras^{V12} in the absence of pRb.

pRb delays N-Ras isoprenylation

To explore the mechanism of N-Ras activation control by pRb, we transduced AC61 cells with moderately expressed pRb using titer-known retrovirus (multiplicity of infection at 1.0). We then transiently transduced these cells with the monomeric-Venus^{A207R}-tagged N-Ras (Venus-N-Ras). The higher molecular weight endowed by tagging provided us with a better separation of proteins during SDS-PAGE. In addition, rapid analysis immediately after completing transfection and under optimal conditions enabled us to detect cytosolic (unprenylated) Venus-N-Ras proteins on IB and image analyses before the majority of them become isoprenylated. In cells growing in 10% FBS, the moderate expression of pRb attenuated Venus-N-Ras activity to almost half (Figure 5B). However, under this condition, the difference in the migration degree of Venus-N-Ras was barely noticeable. When we decreased FBS to 0.5% in an attempt to enhance pRb activity, we observed an increased proportion of the unprenylated form only in the presence of pRb. Under this condition, the majority of pRb was hypophosphorylated. This effect of pRb was comparable to that of prenyltransferase inhibitors (PTIs), and was reversed by 1

hr serum restimulation. However, Venus-N-Ras activation upon serum restimulation was significantly delayed in the presence of pRb or PTIs (Figure 5B). We observed the same effect of pRb on N-Ras isoprenylation in another *Rb*-deficient *N-ras*$^{-/-}$ cell line (AC62) (Figure 5C). These findings suggest that pRb delays N-Ras isoprenylation and activation.

pRb downregulates membrane trafficking of N-Ras

We observed an increased proportion of unprenylated N-Ras on IB in pRb-positive cells only when cultured under low serum conditions. N-Ras in the isoprenylated fractions include not only those anchored to the plasma membrane, but also those anchored to endomembranes such as Golgi, ER and other vesicles. Thus, a considerable proportion of N-Ras are membrane-anchored but not always activated. Therefore, we next investigated the effects of pRb on subcellular localization of N-Ras. We cotransfected Venus-N-Ras and red fluorescent protein (RFP)-tagged Rab6A (RFP-Rab6A) as a Golgi marker without the CAAX motif (Goud et al., 1990). Twelve hours after transfection in 10% FBS, Venus-N-Ras overlapping with RFP-Rab6A became detectable in both pRb-negaive and positive cells (Figure 5D). From then, we decreased FBS concentration to 0.1% for 12 hr and observed that the signal overlap was barely detectable in pRb-positive cells, whereas it was readily detectable in pRb-negative cells. The abundance and subcellular localization of RFP-Rab6A were not affected by pRb status nor by serum depletion. PTIs exhibited the same

effect as pRb during serum depletion. Under these conditions (0.1% FBS for 12 hr), we observed that in the absence of pRb, about half of the Venus-N-Ras was isoprenylated and enriched in the membrane fraction, whereas in the presence of pRb, most of the Venus-N-Ras was still unprenylated and remained in the cytosolic fraction (Figure 5D). After 18 hr serum depletion, we observed a slight recovery in the signal overlap in pRb-positive cells. Serum restimulation enabled the recovery of signal overlap to the initial level after 2 hr (Figure 5D). These findings suggest that the serum concentration influences the pRb function in reducing N-Ras in Golgi at a particular time point. Disappearance of Venus-N-Ras from Golgi can be explained by downregulated transport to Golgi due to the decreased isoprenylation.

Next, to examine whether delayed membrane trafficking attenuates N-Ras activation, we observed AC61 cells cotransfected with Venus-N-Ras and RFP-Rab6A using a confocal laser microscope. After 24 hr culture in 10% FBS and subsequent 48 hr culture in 0.1% FBS, the overlap of Venus-N-Ras and RFP-Rab6A signals was significantly higher in pRb-negative than pRb-positive cells, however, the Venus-N-Ras signal was not detectable at the plasma membrane in both cells (Figure 5E and S7). Notably, 10 min after serum restimulation, a strong Venus-N-Ras signal was detected in the periphery of pRb-negative, but not pRb-positive cells (Figure 5E and S7). These observations suggest that pRb delays Venus-N-Ras transport to Golgi by attenuating endomembrane anchoring

and thereby delays further trafficking to the plasma membrane. We further speculated that N-Ras-induced cellular senescence in *Rb*-deficient C-cells depends on isoprenylation, as the N-Ras^{SAAX} (N-Ras^{S186}) mutant that cannot be isoprenylated completely failed to induce DDR and cellular senescence in AC61 cells (Figure 5F) or to suppress colony formation by *Rb*$^{-/-}$;*N-ras*$^{-/-}$ MEFs (data not shown). Similarly, treatment with PTIs significantly suppressed N-Ras-induced DDR and cellular senescence in AC61 cells (Figure 5G). We finally examined whether *Rb*-loss increases N-Ras isoprenylation. Venus-N-Ras was introduced into *Rb*$^{+/+}$ and *Rb*$^{-/-}$ MEFs. Upon serum starvation, started 8 hr after transfection, *Rb*$^{-/-}$ MEFs exhibited faster isoprenylation of Venus-N-Ras protein compared to littermate *Rb*$^{+/+}$ MEFs (Figure 5H and S8), suggesting that *Rb*-loss in MEFs accelerates N-Ras isoprenylation.

pRb downregulates genes involved in isoprenylation

A previous study demonstrated that the influence of pRb on Ras activity depended on *de novo* protein synthesis (Lee et al, 1999). We therefore performed microarray analysis on AC61 cells freshly transduced with moderately expressed pRb. These cells were maintained unsynchronized in 10% FBS, which allowed the cells to attenuate N-Ras activity to half (Figure 5B). Genes significantly upregulated by pRb included many cell surface antigens, lymphokines, interferons and inflammation-related genes (Figure S9), similar to previous results obtained by analyzing MEFs conditionally lacked pRb (Markey

et al., 2007). Moreover, in genes significantly downregulated by pRb, we detected known E2F-target genes such as *Cdc6*, *N-myc* and *Mmp-3* with the highest statistical significance (change p-value >0.99998 determined by Wilcoxon's signed rank test), suggesting that pRb reconstitution was successful (Table S1).

In 396 significantly upregulated genes (change p-value <0.001), we did not detect genes that could be directly involved in suppressing Ras activity such as *GTPase activating protein*. In 270 significantly downregulated genes (change p-value >0.9998), we found that *farnesyl diphosphate farnesyl transferase 1* (*Fdft1*) had the highest rank (Table S1). In addition, we detected number of genes (Table S2) predicted to be transactivated by SREBPs via sterol regulatory element (SRE) (Sakakura et al., 2001). Other genes that could be directly involved in stimulating Ras activation, such as *GTP-exchange factor* or *receptor tyrosine kinase* were not detected. We then analyzed pRb-reconstituted AC61 cells by RT-PCR. Surprisingly, in addition to *Fdft1*, *farnesyl diphosphate synthase* (*Fdps*) (Szkopinska and Plochocka, 2005), most of the prenyltransferases (*Fnta*: *farnesyltransferase* α, *Fntb*: *farnesyltransferase* β, *Pggt1b*: *protein geranylgeranyltransferase* 1β and *Rabggtb*: *Rab geranylgeranyltrasferase* β) (Maurer-Stroh et al., 2003) and *SREBP-1, SREBP-2* were significantly downregulated by pRb. All these genes were induced in MEFs following *Rb*-loss or pRb inactivation using SV40 large T antigen or

adenovirus E1A (Figure 6A). A farnesyltransferase β immunoblot validated the results of the RT-PCR (Figure 6B). We did not detect a significant change in *NF1* (Courtois-Cox et al., 2006) expression (data not shown).

To investigate the *in vivo* relevance of the increased expression of genes involved in protein isoprenylation in *Rb*-deficient cells, primary *Rb*-deficient C-cell adenomas were immunohistochemically analyzed. These tumors expressed significantly higher levels of Fntb, SREBP-1 and SREBP-2 compared to normal thyroid tissue (Figure 6C). We then compared expression level of these proteins between pRb-positive *ret* mutation-positive human medullary thyroid carcinoma (C-cell) cell line TT (Tomoda et al., 2008) and AC61. AC61 cells expressed significantly higher levels of Fnta, Fntb and SREBP-1, SREBP-2 compared to TT cells (Figure S10).

E2F-dependent transcription control of genes involved in isoprenylation

To further investigate the mechanism by which pRb controls genes involved in protein isoprenylation, we analyzed the promoter regions of these genes. We detected several E2F-binding consensus sequences in the promoter regions of *SREBPs* (Figure S11). Moreover, we detected several E2F-binding consensus sequences in each of the promoters of *Fdps* and *prenyltransferases*. These findings suggest that E2Fs control *Fdps* and *prenyltransferases* via a dual mechanism involving SREBPs and direct binding. ChIP assay detected the

direct binding of E2F-1 and E2F-3 to the promoters of these genes specifically in the absence of pRb (Figure 6D). E2F-3 exhibited stronger DNA binding activity to the *Fntb* promoter than E2F-1. We also detected direct binding of pRb to the *Fdps* promoter. pRb prevented SREBPs binding to the *Fdps* promoter, probably via downregulation of *SREBPs*. Further, a pRb mutant derived from a retinoblastoma and lacking the ability to attenuate Ras activation (Lee et al., 1999) could not bind to the *Fdps* promoter and did not suppress SREBPs binding. However, a partially penetrant mutant pRb (Sellers et al., 1998) with the ability to attenuate Ras activation (Lee et al., 1999) bound to the *Fdps* promoter and suppressed SREBPs binding (Figure S12), suggesting that the function of pRb to attenuate Ras activation is not separable from its ability to regulate the *Fdps* promoter and SREBPs.

Fdps, *Fntb* and *SREBP-1* promoters were downregulated by pRb. This effect was augmented by serum depletion. These promoters were upregulated by either E2F-1 or E2F-3 (Figure 6E). In particular, E2F-3 was more potent than E2F-1 in transactivating the *Fntb* promoter, in agreement with the ChIP results (Figure 6D). The truncated mutant E2F containing the DNA-binding domain but lacking the transactivation domain (E2F-DB) slightly, but significantly, downregulated these promoters, suggesting the involvement of liberated E2Fs in the basal transactivation. Except for the *Fntb* promoter, which lacks SRE, *Fdps* and *SREBP-1* promoters were upregulated by SREBP-1c. The dominant

negative SREBP-1c downregulated the basal transactivation of these two promoters, indicating increased endogenous SREBP activity in AC61 cells. Further, these three promoters were downregulated by pRb in two other pRb-negative cells (*Rb*$^{-/-}$;*N-ras*$^{-/-}$ MEFs and Saos2). Transduction of E2F-DB, SV40 large T antigen or adenovirus E1A in MEFs induced *Fdps* promoter transactivation (Figure 6E). E2F-DB is known to affect the functions of E2Fs in multiple ways: one is to derepress active transcriptional silencing by the pRb-E2F complex (Rowland et al., 2002). Thus, we considered that the pRb-E2F complex directly participates in the transcriptional repression of *Fdps*.

pRb-dependent protein farnesylation

The CAAX motif constitutes a C-terminal tetrapeptide common to all Ras, directing multi-step post-translational modifications initiated by farnesyl transferases (Hancock, 2003). There are approximately 300 proteins with the CAAX motif that are potentially farnesylated. To investigate pRb's effects on these proteins, we analyzed AC61 cells or MEFs that were metabolically labeled with [^{3}H]farnesol. In 10% FBS, pRb-negative cells showed an increased density of farnesylated protein bands. When serum was depleted, this difference became higher (Figure 6F and S13). These findings suggest that *Rb*-loss induces enhanced global protein farnesylation.

Clinical relevance of pRb-N-Ras pathway in MTCs

Human medullary thyroid carcinomas (MTCs) are pathologically similar to C-cell adenocarcinomas in the mice analyzed in this study. Human C-cell adenoma is extremely rare. Familial MTCs are frequently associated with mutation in the *ret* oncogene, however, almost half of sporadic MTCs are free of the *ret* mutation (Marsh et al., 2003) indicating the *ret*-independent mechanism involved in human C-cell carcinogenesis. To address the relevance of the pRb-N-Ras pathway in human tumors, we analyzed 13 sporadic MTCs, of which, 6 cases (46%) were immunohistochemically negative for pRb and 7 cases (54%) were negative for N-Ras (Figure 7A). Notably, 6 of 7 N-Ras-negative tumors were negative for pRb (Figure 7B). This finding in human is consistent with the requirement of N-Ras suppression in *Rb*-deficient C-cell carcinogenesis in mice.

Discussion

The current work has provided evidence that in the absence of pRb, E2F-1 and E2F-3 participate in the transactivation of most of the genes involved in protein isoprenylation either directly or via SREBPs. This at least partially explains Ras activity elevation induced by pRb inactivation (Figure S14A). It would be of interest to ascertain whether under physiological conditions, Ras and pRb activities oscillate due to the mutual suppression via cyclinD/Cdk4/6 and E2F/isoprenylation (Figure S14B). Further, this study partially clarified the mechanism of the tumor suppressor function of wild-type Ras. It has previously

been shown that loss of the normal *ras* allele, in addition to activating mutation, was required for tumorigenesis (refs in Zhang et al., 2001). This study indicated that N-Ras and N-Ras^{V12} exert different functions in *Rb*-deficient cells where only N-Ras can induce p130-dependent cellular senescence, which explains why N-Ras ^{V12} requires pRb to induce cellular senescence.

Cell cycle-dependent Ras activation was noted by Taylor and Shalloway (1997). Later, it was discovered that pRb inactivation (Raptis et al., 1997) or genetic loss (Lee et al., 1999) elevates Ras activity. The latter study observed that high N-Ras activation was sharply induced in serum starved *Rb*$^{-/-}$ MEFs only 10 min after serum restimulation. We suspect that during serum starvation, pRb-negative cells pool greater numbers of N-Ras-GDP molecules in space where GDP to GTP exchange readily occurs upon serum restimulation. Indeed, our results suggest that isoprenylated Ras-GDP proteins are aberrantly enriched in the Golgi complex in pRb-negative cells during serum starvation. At Golgi, Ras is activated through src-mediated activation of phospholipase Cγ. The nature of Ras signaling generated from Golgi is supposed to be distinct from that generated from plasma membrane in terms of activation of JNK, ERK, AKT and Ral pathways (Hancock, 2003; Quatela and Philips, 2006). Therefore, in addition to moderate level activation, enrichment of N-Ras in Golgi in *Rb*-deficient cells may assign a specific role to itself.

Simultaneous *N-ras* or *K-ras* deletion rescues differentiation defects in *Rb*-null embryos and prolongs life span with no detectable impact on E2F-dependent ectopic proliferation and apoptosis (Takahashi et al., 2003; Takahashi et al., 2004). This is in line with our observation that the isoprenylation-dependent regulation of Ras activation is genetically downstream of E2Fs in the absence of pRb (Figure S14A). The limited effect of E2Fs deletion on differentiation defects in $Rb^{-/-}$ embryos can be explained by the redundant functions shared by E2F family members. Indeed, deletion of individual E2F in $Rb^{-/-}$ embryos resulted in varying degrees of rescue of erythropoiesis (Wikenheiser-Brokamp, 2006; Dirlam et al., 2007). The extended life span in *Rb*-deficient embryos achieved by additionally deleting *N-ras* was obviously due to the rescue of hepatic anemia (Takahashi et al., 2003). Although the etiology of *Rb*-deficient anemia is still controversial, a significant genetic interaction seems to exist between *E2Fs* and *N-ras* in *Rb*-mediated erythropoiesis. Furthermore, common C-cell tumor phenotypes in $Rb^{+/-}$;$E2F\text{-}3^{-/-}$ and $Rb^{+/-}$;$N\text{-}ras^{-/-}$ mice, the senescence-inducing activity of E2F-3 *in vivo* (Lazzerini Denchi et al., 2005) and the role of E2F-3 in regulating the transcription of genes involved in Ras isoprenylation (this study) suggest that *E2F-3* and *N-ras* are genetically linked in *Rb*-deficient C-cell carcinogenesis.

Our observation of less frequent senescence markers, compared to DDR, in

early *Rb*-deficient adenomas indicates that chronologically DDR precedes the appearance of senescence markers during adenoma formation. However, this does not necessarily mean that *Rb*-loss-induced DNA damage is a prerequisite for inducing cellular senescence. To further address this issue, we are analyzing $Rb^{+/-}$;$ATM^{-/-}$ mice (AS and CT unpublihsed). The RB pathway has been linked to DDR through E2F-dependent pathways (Pickering and Kowalik, 2006) involving cyclin E (Tort et al., 2006) or Mad2 (Hernando et al., 2004). Our study proposes that N-Ras or other isoprenylated proteins may participate in accumulating DNA double strand breaks in *Rb*-deficient cells.

This study also elucidates the tumor suppressor roles of p130, $p16^{INK4a}$, ARF and Suv39H1 in the absence of pRb. Despite the role of p53 in human retinoblastoma, $Rb^{+/-}$;$p53^{+/-}$ mice produce C-cell adenocarcinoma at a lower frequency (8%) following spontaneous mutation in the *ret* oncogene (Coxon et al., 1998) compared to $Rb^{+/-}$;$N\text{-}ras^{-/-}$ mice (91.6 %). This suggests that particularly in C-cells, the lower p53 activity acts independently to increase genomic instability rather than intimately cooperating with the pRb pathway.

This study also explains the tumor-promoting function of wild-type Ras observed in *Rb*-deficient pituitary glands (Takahashi et al., 2004; Takahashi et al., 2006) and immortalized fibroblasts (Raptis et al., 1997; Fotiadou et al., 2007). OIS is known to occur in limited cell types, but activated Ras promotes carcinogenesis

in many cell types. Further, not only Ras but also other isoprenylated proteins such as Ras2, RhoA, RhoB, RhoC, RhoE, Rac1, Rac2, Cdc42, Rheb, TC10, TC21, RalA, Rap1A, Rap1B, Rap2, Rab8, Rab11, Rab13, CENP-E, CENP-F (Maurer-Stroh et al., 2003) may be orchestrated by pRB via E2Fs. We have previously detected upregulated RhoA, Rac and Cdc42 activities in *Rb*-deficient cells (Takahashi et al., 2006). Finally, we emphasize that our study provides rational basis for applying PTIs to pRB-inactivated tumors without somatic *ras* mutations such as retinoblastoma, osteosarcoma and small cell lung carcinoma.

Experimental procedures

Animals

Rb$^{+/-}$ mice with various *N-ras* genotypes were described (Takahashi et al., 2006). *Rb*$^{+/-}$ mice were crossed with *Ink4a*$^{-/-}$, *ARF*$^{-/-}$, *Ink4a*$^{-/-}$;*ARF*$^{-/-}$ or *Suv39H1*$^{-/-}$ mice, and the resultant progeny was intercrossed to generate mice used in this study. Average age at examination (AE) was determined irrespective of the mouse status. Mouse genotyping is described in Supplemental Experimental Procedures. The protocol of this study was approved by the ethical committee of Kyoto University Graduate School of Medicine, and animals were handled in accordance with the guidelines of Kyoto University.

Cell Culture

Primary C-cell adenocarcinoma cell lines were established as described (Takahashi et al., 2006) with minor modifications. MEFs were prepared from E12.5 embryos derived by intercrossing *Rb*$^{+/-}$;*N-ras*$^{+/-}$ or *Rb*$^{+/-}$;*Ink4a*$^{+/-}$ mice.

Comet Assay

CometAssay Reagent Kit was purchased from Trevigen (4250-050K).

RNA Interference

MISSION TRC shRNA target sets (TRCN0000071271, 71274 for p130 and 34391, 34392, 34393 for N-Ras) and TurboGFP shRNA control vector (SHC004) were purchased from Sigma-Aldrich.

BrdU incorporation

BrdU incorporation was measured as described previously (Takahashi et al., 2004).

Colony Formation Assays

Colony formation was assessed by plating 1.0 x 10^3 cells per 60 mm dish. After 14 days cultivation, giemsa staining was used to visualize colonies. Suppression of colony formation was observed by transfecting 1.0 x 10^5 MEFs with 0.5 μg pLXSB and 5 μg pBabe-puro expressing the indicated proteins, followed by 14

days cultivation with 8 μg/ml blasticidin S.

Ras Activation Assay

Pull-down assay to measure N-Ras activity was performed as described previously (Lee et al., 1999).

Prenylation Assay

Cells transiently transfected with pCAGGS-Venus^{A207R}-N-Ras were lysed as described (Miki et al., 2007), sonicated for 3 cycles of 15 s each, and separated on 8~10 % acrylamide SDS-PAGE gel at a low constant voltage (less than 40 V for longer than 36 h). FTI-I (#344150), FTI-277 (#344555) and GGTI-298 (#345883) were purchased from Calbiochem.

RT-PCR

Total RNA was extracted using RNeasy Mini Kit from Qiagen (74104) and RT-PCR was performed using TaKaRa RNA PCR Kit (RR019A) and the sequence specific primers indicated in Table S3.

Chromatin Immunoprecipitation

ChIP reagents (SC-45000, 45001, 45002 and 45003) were purchased from Santa Cruz Biotechnology. Lysates were immunoreacted with specific antibodies. Released DNA was amplified by PCR using the primers indicated in Table S4.

Global Farnesylation Assay

5 x 10^6 cells were cultured in 10% FBS with 10 mM Lovastatin for 4 hr. After removing Lovastatin, the cells were incubated with 1.54 MBeq [^{3}H]farnesol in the presence of 10% FBS for 4 hr and then in the presence of 10% or 0.5% FBS for additional 20 hr. Labeled proteins were analyzed as described previously (Andreas et al., 1999).

Human Tumor

Tumors from patients with MTC were surgically removed at the Department of Endocrine Surgery and diagnosed at the Department of Pathology, Tokyo Women's Medical University. The protocol of this study was approved by the ethical committee of Tokyo Women's Medical University and informed consent was obtained from all patients.

SUPPLEMENTAL DATA

Supplemental Data include Experimental Procedures, references, 14 figures and 4 tables.

Microarray data

Microarray data are deposited at:

http://www.ncbi.nlm.nih.gov/projects/geo/query/acc.cgi?acc=GSE12637.

Acknowledgments

We thank M. Ewen for encouragement and reagents, D. Peeper and T. Taguchi for discussion and reagents, T. Noda and Y. Saiki for critical reading of the manuscript, A. Iwama, T. Jacks, T. Jenuwein, T. Kamijo, R. Kucherlapati, M. Serrano, N. Sharpless and M. Taketo for animals, S. Gaubatz, W. Hahn, M. Madiredjo, M. Matsuda, W. Sellers and B. Spiegelman for reagents, H. Futami, Y. Murakami, T. Nishikawa, S. Ogawa and R. Takahashi for help in analyzing tumors, A. Nishimoto, H. Gu and A. Miyazaki for assistance, and K. Lee for inspiring. This work was supported by Research Grant of the Princess Takamatsu Cancer Research Fund, Takeda Science Foundation, and Japan Ministry of Education, Culture, Sports, Science and Technology.

References

Andreas, D. A., Crick, D. C., Finlin, B. S., and Waechter, C. J. (1999). Rapid identification of cycteine-linked isoprenoyl groups by metabolic labeling with [3H]Farnesol and [3H]geranylgeranoil. In Protein Lipidation Protocols, M. H. Gelb, ed. (New Jersey: Humana Press), 107-123.

Ceol, C. J., and Horvitz, H. R. (2001). dpl-1 DP and efl-1 E2F act with lin-35 Rb to antagonize Ras signaling in C. elegans vulval development. Mol Cell 7, 461-

473.

Chen, Z., Trotman, L. C., Shaffer, D., Lin, H. K., Dotan, Z. A., Niki, M., Koutcher, J. A., Scher, H. I., Ludwig, T., Gerald, W., et al. (2005). Crucial role of p53-dependent cellular senescence in suppression of Pten-deficient tumorigenesis. Nature 436, 725-730.

Collado, M., Blasco, M. A., and Serrano, M. (2007). Cellular senescence in cancer and aging. Cell 130, 223-233.

Cortois-Cox, S., Genther Williamns, S. M., Reczeke, E. E., Johnson, B. W., McGillicuddy, L. T., Johannessen, C. M., Holsten, P. E., MacCollin, M., and Cichowski, K. (2006). A negative feedback signaling network underlies oncogene-induced senescence. Cancer Cell 10, 459-472.

Coxon, A. B., Ward, J. M., Geradts, J., Otterson, G. A., Zajac-Kaye, M., and Kaye, F. J. (1998). RET cooperates with RB/p53 inactivation in a somatic multi-step model for murine thyroid cancer. Oncogene 17, 1625-1628.

Di Micco, R., Fumagalli, M., and di Fagagna, F. (2007). Breaking news: high-speed race ends in arrest--how oncogenes induce senescence. Trends Cell Biol 17, 529-536.

Dimri, G. P. (2005). What has senescence got to do with cancer? Cancer Cell 7, 505-512.

Dirlam, A., Spike, B. T., and Macleod, K. F. (2007). Deregulated E2f-2 underlies cell cycle and maturation defects in retinoblastoma null erythroblasts. Mol Cell Biol 27, 8713-8728.

Fotiadou, P. P., Takahashi, C., Rajabi, H. N., and Ewen, M. E. (2007). Wild-type NRas and KRas perform distinct functions during transformation. Mol Cell Biol 27, 6742-6755.

Goud, B., Zahraoui, A., Tavitian, A., and Saraste, J. (1990). Small GTP-binding protein associated with Golgi cisternae. Nature 345, 553–556.

Hancock, J. F. (2003). Ras proteins: different signals from different locations. Nat Rev Mol Cell Biol 4, 373-384.

Hernando, E., Nahle, Z., Juan, G., Diaz-Rodriguez, E., Alaminos, M., Hemann, M., Michel, L., Mittal, V., Gerald, W., Benezra, R., et al. (2004). Rb inactivation promotes genomic instability by uncoupling cell cycle progression from mitotic control. Nature 430, 797-802.

Laurie, N. A., Donovan, S. L., Shih, C. S., Zhang, J., Mills, N., Fuller, C., Teunisse, A., Lam, S., Ramos, Y., Mohan, A., et al. (2006). Inactivation of the p53 pathway in retinoblastoma. Nature 444, 61-66.

Lazzerini Denchi, E., Attwooll, C., Pasini, D., and Helin, K. (2005). Deregulated E2F activity induces hyperplasia and senescence-like features in the mouse pituitary gland. Mol Cell Biol 25, 2660-2672.

Lee, K. Y., Ladha, M. H., McMahon, C., and Ewen, M. E. (1999). The retinoblastoma protein is linked to the activation of Ras. Mol Cell Biol 19, 7724-7732.

Markey, M. P., Bergseid, J., Bosco, E. E., Stengel, K., Xu, H., Mayhew, C. N., Schwemberger, S. J., Braden, W. A., Jiang, Y., Babcock, G. F., et al. (2007). Loss of the retinoblastoma tumor suppressor: differential action on transcriptional programs related to cell cycle control and immune function. Oncogene 26, 6307-6318.

Marsh, D. J., Theodosopoulos, G., Martin-Schulte, K., Richardson, A. L., Philips, J., Roher, H. D., Delbridge, L., and Robinson, B. G. (2003). Genome-wide copy number imbalances identified in familial and sporadic medullary thyroid

carcinoma. J Clin Endocrinol Metab 88, 1866-1872.

Maurer-Stroh, S., Washietl, S., and Eisenhaber, F. (2003). Protein prenyltransferases. Genome Biol 4, 212.

Miki, T., Takegami, Y., Okawa, K., Muraguchi, T., Noda, M., and Takahashi, C. (2007). The reversion-inducing cysteine-rich protein with Kazal motifs (RECK) interacts with membrane type 1 matrix metalloproteinase and CD13/aminopeptidase N and modulates their endocytic pathways. J Biol Chem 282, 12341-12352.

Mooi, W. J., and Peeper, D. S. (2006). Oncogene-induced cell senescence--halting on the road to cancer. N Engl J Med 355, 1037-1046.

Narita, M., Nunez, S., Heard, E., Narita, M., Lin, A. W., Hearn, S. A., Spector, D. L., Hannon, G. J., and Lowe, S. W. (2003). Rb-mediated heterochromatin formation and silencing of E2F target genes during cellular senescence. Cell 113, 703-716.

Peeper, D. S., Upton, T. M., Ladha, M. H., Neuman, E., Zalvide, J., Bernards, R., DeCaprio, J. A., and Ewen, M. E. (1997). Ras signalling linked to the cell-cycle machinery by the retinoblastoma protein. Nature 386, 177-181.

Pickering, M. T., and Kowalik, T. F. (2006). Rb inactivation leads to E2F1-mediated DNA double-strand break accumulation. Oncogene 25, 746-755.

Quatela, S. E., and Philips, M. R. (2006). Ras signaling on the Golgi. Curr Opin Cell Biol 18, 162-167.

Raptis, L., Brownell, H. L., Corbley, M. J., Wood, K. W., Wang, D., and Haliotis, T. (1997). Cellular ras gene activity is required for full neoplastic transformation by the large tumor antigen of SV40. Cell Growth Differ 8, 891-901.

Rowland, B. D., Denissov, S. G., Douma, S., Stunnenberg, H. G., Bernards, R., and Peeper, D. S. (2002). E2F transcriptional repressor complexes are critical downstream targets of p19(ARF)/p53-induced proliferative arrest. Cancer Cell 2, 55-65.

Sage, J., Mulligan, G. J., Attardi, L. D., Miller, A., Chen, S., Williams, B., Theodorou, E., and Jacks, T. (2000). Targeted disruption of the three Rb-related genes leads to loss of G(1) control and immortalization. Genes Dev 14, 3037-3050.

Sakakura, Y., Shimano, H., Sone, H., Takahashi, A., Inoue, N., Toyoshima, H.,

Suzuki, S., and Yamada, N. (2001). Sterol regulatory element-binding proteins induce an entire pathway of cholesterol synthesis. Biochem Biophys Res Commun 286, 176-183.

Sellers, W. R., Novitch, B. G., Miyake, S., Heith, A., Otterson, G. A., Kaye, F. J., Lassar, A. B., and Kaelin, W. G., Jr. (1998). Stable binding to E2F is not required for the retinoblastoma protein to activate transcription, promote differentiation, and suppress tumor cell growth. Genes Dev 12, 95-106.

Shiloh, Y. (2003). ATM and related protein kinases: safeguarding genome integrity. Nat Rev Cancer 3, 155-168.

Szkopinska, A., and Plochocka, D. (2005), Farnesyl diphophate synthase; regulation of product specificity. Acta Biochim Polonica 52, 45-55.

Takahashi, C., Bronson, R. T., Socolovsky, M., Contreras, B., Lee, K. Y., Jacks, T., Noda, M., Kucherlapati, R., and Ewen, M. E. (2003). Rb and N-ras function together to control differentiation in the mouse. Mol Cell Biol 23, 5256-5268.

Takahashi, C., Contreras, B., Bronson, R. T., Loda, M., and Ewen, M. E. (2004). Genetic interaction between Rb and K-ras in the control of differentiation and tumor suppression. Mol Cell Biol 24, 10406-10415.

Takahashi, C., Contreras, B., Iwanaga, T., Takegami, Y., Bakker, A., Bronson, R. T., Noda, M., Loda, M., Hunt, J. L., and Ewen, M. E. (2006). Nras loss induces metastatic conversion of Rb1-deficient neuroendocrine thyroid tumor. Nat Genet 38, 118-123.

Taylor, S. J., and Shalloway, D. (1996). Cell cycle-dependent activation of Ras. Curr Biol 6, 1621-1627.

Todaro, G. J., and Green, H. (1963). Quantitative studies of the growth of mouse embryo cells in culture and their development into established lines. J Cell Biol 17, 299-313.

Tomoda, C., Moatamed, F., Naeim, F., Hershman, J. M., and Sugawara, M. (2008). Indomethacin inhibits cell growth of medullary thyroid carcinoma by reducing cell cycle progression into s phase. Exp Biol Med (Maywood) 233, 1433-1440.

Tort, F., Bartkova, J., Sehested, M., Orntoft, T., Lukas, J., and Bartek, J. (2006). Retinoblastoma pathway defects show differential ability to activate the constitutive DNA damage response in human tumorigenesis. Cancer Res 66, 10258-10263.

Tsai, K. Y., Hu, Y., Macleod, K. F., Crowley, D., Yamasaki, L., and Jacks, T. (1998). Mutation of E2f-1 suppresses apoptosis and inappropriate S phase entry and extends survival of Rb-deficient mouse embryos. Mol Cell 2, 293-304.

Wikenheiser-Brokamp, K. A. (2006). Retinoblastoma family proteins: insights gained through genetic manipulation of mice. Cell Mol Life Sci 63, 767-780.

Young, A. P., Schlisio, S., Minamishima, Y. A., Zhang, Q., Li, L., Grisanzio, C., Signoretti, S., and Kaelin, W. G., Jr. (2008). VHL loss actuates a HIF-independent senescence programme mediated by Rb and p400. Nat Cell Biol 10, 361-369.

Zhang, Z., Wang, Y., Vikis, H. G., Johnson, L., Liu, G., Li, J., Anderson, M. W., Sills, R. C., Hong, H. L., Devereux, T. R., et al. (2001). Wild-type Kras2 can inhibit lung carcinogenesis in mice. Nat Genet 29, 25-33.

Ziebold, U., Lee, E. Y., Bronson, R. T., and Lees, J. A. (2003). E2F3 loss has opposing effects on different pRB-deficient tumors, resulting in suppression of pituitary tumors but metastasis of medullary thyroid carcinomas. Mol Cell Biol 23, 6542-6552.

Figure legends

Figure 1. Analysis of C-cell tumors in *Rb*$^{+/-}$;*N-ras*$^{+/+}$ and *Rb*$^{+/-}$;*N-ras*$^{-/-}$ mice.

(A) Scheme of C-cell carcinogenesis in *Rb*$^{+/-}$ mice drawn based on previous findings.

(B) Immunohistochemical (IHC) analysis and SA-β-gal assay of thyroid and C-cell tumors in mice with the indicated genotypes. 22 *Rb*$^{+/-}$;*N-ras*$^{+/+}$ (AE = 11.0 ± 1.2) and 28 *Rb*$^{+/-}$;*N-ras*$^{-/-}$ (AE = 10.6 ± 0.9) mice were analyzed. Scale bars: 100 μm. The frequency of immuno-stain positive cells per 200 normal thyroid or tumor cells is quantified. Columns are mean + SE.

Figure 2. C-cell tumor phenotypes in *Rb*$^{+/-}$ mice additionally lacking senescence-mediating genes.

(A) C-cell tumors (indicated by arrows) developed in mice with the indicated genotype and age (months). Scale bars: 3 mm.

(B) Histological and IHC analysis of C-cell tumors developed in mice with the indicated genotype and age. Scale bars: 100 μm.

(C) Calcitonin staining of cultured tumor cells prepared from thyroids of mice with the indicated genotype. Scale bars: 100 μm.

Figure 3. Effects of N-Ras reconstitution in *Rb*-deficient *N-ras*$^{-/-}$ C-cell adenocarcinoma.

(A) Immunoblot (IB) analysis of TT and AC61 cells infected with pBabe-puro (vector) or pBabe-puro-N-ras for the indicated proteins (top). Histological and IHC analysis of AC61 cells infected with pBabe-puro or pBabe-puro-N-ras, selected, and cultured subcutaneously in BALB/c-*nu*/*nu* mice for 14 days (middle). Primary C-cell tumors from mice of the indicated genotype are illustrated (bottom). Scale bars: 100 μm. Tumor weights and frequency of immuno-stain positive cells per 200 tumor cells are quantified (right). Columns are mean + SE from 4 tumors each.

(B) Immunofluorescence (IF) analysis of AC61 cells infected with pBabe-puro vectors expressing the indicated proteins, selected, and cultured for additional 8 days. Blue signals: DAPI. Scale bars: 10 μm.

(C) Comet assay of cells from (B). Scale bars: 30 μm. Cells with DNA double strand breaks per 200 cells are quantified. Numbers are mean ± SE from 3 experiments.

(D) IF analysis of cells prepared as in (B) and cultured for additional 12 days. Scale bars: 10 μm.

(E) IB of acid-extracted (γH2AX, Suv39h1, H3K9me3, HP1γ) or whole cell lysates (others) from cells prepared as in (B) and cultured for additional 9 days. NT: non-treated, H_2O_2: treated with 200 μM H_2O_2 for 30 min at 4 ^{o}C, SS: serum starved in 0.1% FBS for 24 hr.

(F) AC61 cells were infected with pBabe-puro vectors expressing the indicated proteins, and selected (upper). AC61 cells infected with pLXSB or pLXSB-Rb, and selected were re-infected with pBabe-puro vectors expressing the indicated proteins, and selected (lower). Cell proliferation was monitored from day 6 onwards and SA-β-gal activity was detected at day 11 after the last infection. Scale bars: 30 μm.

(G) Immunoprecipitation (IP) from whole cell lysates (WCL) or chromatin fraction (CH) of cells prepared as in (B) and cultured for additional 9 days (left). HP1γ bound to p130 or Suv39h1 in the chromatin fraction are the upper bands. Colocalization of p130 and HP1γ in these cells is demonstrated (right). Scale bars: 5 μm.

(H) AC61 cells were infected with lentivirus expressing the indicated shRNAs, and selected with puromycin. Five days after the initial infection, cells were re-infected with pLXSB or pLXSB-N-ras, selected, and analyzed. BrdU incorporation determined by FACS and IB at day 6 after the last infection are shown. Bars are mean + SE from dupilcate experiments.

(I) AC61 cells were transduced with the indicated shRNAs 14 days after N-Ras transduction and analyzed as in (H). Bars are mean + SE from dupilcate experiments.

(J) IHC analysis of thyroids or primary C-cell tumors developed in mice of the indicated genotypes. Scale bars: 100 μm. Quantification was performed as in (A). Columns are mean + SE (n ≥20 each).

Figure 4. *Rb-N-ras* genetic interaction in MEFs.

(A) 3T3 protocol assay of MEFs with the indicated genotypes. Cumulative multiplicity in the representative cultures at the indicated passage number is shown.

(B) Representative results of colony formation assays of MEFs with the indicated genotypes plated at low density. Results are quantified. Bars are mean + SE (n = 6).

(C) $Rb^{-/-}$ MEFs infected with lentivirus expressing the indicated shRNAs, selected, plated at low density, re-infected every 5 days for 3 times, and cultured for 21 days from the initial infection (top). IB analysis of cells infected one time with the indicated lentiviruses is shown (bottom).

(D) Colony suppression assay of MEFs with the indicated genotypes cotransfected with pLXSB and pBabe-puro vectors expressing the indicated proteins, and selected. Bars are mean + SE (n = 4).

(E) SA-β-gal assay of MEFs with the indicated genotypes infected with pBabe-puro vectors expressing the indicated proteins, selected, and cultured for 9 days. Scale bars: 100 μm.

(F) Proliferation of MEFs with the indicated genotypes infected with pBabe-puro vectors expressing the indicated proteins, or pMIKcys (K-Ras^{V12}). After selection, 1.0 x 10^5 viable cells were plated on 100 mm dish (day 6) and cell number was counted at the indicated time points.

Figure 5. Effects of pRb on N-Ras isoprenylation and membrane trafficking.

(A) AC61 cells transfected with 0.25 μg pBabe-puro-N-ras or pBabe-puro-N-ras^{V12} together with 2.5 μg pSG5 or pSG5L-HA-Rb were selected, and analyzed for GTP-bound N-Ras or status of the indicated proteins in the presence of 10% FBS. Pull down of GTP-loaded N-Ras was done using Glutathione *S*-transferase (GST)-fused Ras-binding domain (RBD) of Raf. N-Ras-GTP/Total ratio in the presence of N-Ras and pRb (lane2) was set to 1.0 (underlined), and relative N-Ras activity in other lanes was estimated.

(B) AC61 cells infected with pLXSB or pLXSB-Rb and selected were transiently transfected with pCAGGS-Venus^{A207R}-N-Ras, treated under the indicated conditions, and analyzed for N-Ras prenylation status (upper 3 cases) and activity (lower 3 cases). PTIs represent the mixture of prenyltranfrase inhibitors (FTI-II, FTI-277 at 10 μM and GGTI-298 at 2 μM). Unprenylated (UP) and prenylated (P) Venus-N-Ras proteins are indicated by arrows. The status of transduced pRb in each condition is indicated (right).

(C) Another *Rb*-deficient *N-ras*$^{-/-}$ C-cell tumor line AC62 was analyzed in 0.5% FBS as in (B).

(D) AC61 cells prepared as in (B) and cotransfected with pCAGGS-Venus^{A207R}-N-Ras (green) and pCXN2-RFP-Rab6A (red) were monitored using fluorescent microscope under the indicated conditions. Scale bars: 40 μm. Merged signals (arrows) are shown (top). Relative intensity of signals in Golgi (RFP-Rab6A-

positive area) was measured using NIH image J 1.4 program and quantified at the indicated time points (lower left). Results are mean ± SE from 90 cells observed in 3 experiments. Cells cultured in 0.1% FBS for 12 hr were lysed and fractionated. C: cytosolic, M: membranous, W: whole cell lysates (lower right).

(E) AC61 cells were cotransfected with 0.25 μg pCAGGS-Venus^{A207R}-N-Ras (green) and 0.25 μg pCXN2-RFP-Rab6A (red) together with 2.5 μg pCMV or pCMV-Rb. Cells were grown in 10% FBS for 24 hr, serum starved in 0.1 % FBS for additional 48 hr, then restimulated with 10% FBS, and analyzed at the indicated time points using a laser confocal fluorescence microscope. Scale bars: 10 μm. Signal intensity of Venus-N-Ras in the cell periphery was measured using NIH image J 1.4 program and quantified from observation of 50 cells each. Bars are mean + SE from 3 experiments.

(F) AC61 cells were transfected with pBabe-puro, pBabe-puro-N-ras or pBabe-puro-N-ras^{S186}, selected and analyzed after 12 days.

(G) AC61 cells were transfected with pBabe-puro or pBabe-puro-N-ras, selected, treated with 2.5 μM FTI-II, 2.5 μM FTI-277 and 0.5 μM GGTI-298 or with vehicle (DMSO), and analyzed as in (F). Amido black stain is shown as a loading control.

(H) Paired MEFs with the indicated genotypes were transfected with Venus-N-Ras for 8 hr, grown under 0.5% FBS for 24 hr or treated with PTIs as in (G), and analyzed. Prenylated and unprenylated fractions of total Venus-N-Ras are quantified. Another pair of MEFs is shown in Figure S8.

Figure 6. E2F-dependent transcriptional control of enzymes involved in protein isoprenylation.

(A) RT-PCR of the indicated genes in AC61 cells infected with pLXSB or pLXSB-Rb, and pBabe-puro or pBabe-puro-N-ras in the indicated combinations and selected, MEFs infected with pBabe-neo-TAg or control vector, $Rb^{+/+}$ and $Rb^{-/-}$ MEFs cultured in 0.1% FBS for 24 hr, or MEFs infected with pBabe-hygro-E1A or vector control and selected. SV40LT: Simian virus 40 large T antigen, E1A: adenovirus E1A.

(B) IB of fanesyltransferase β in AC61 cells expressing the indicated protein and in $Rb^{-/-}$ and $Rb^{+/+}$ MEFs.

(C) IHC analysis of wild-type thyroids and *Rb*-deficient C-cell adenomas. Scale bars: 100 μm. Quantification was done as in Figure 1B.

(D) ChIP assay of the indicated gene promoters in AC61 cells infected with pLXSB or pLXSB-Rb. Positions and sequences of the primers in mouse genome are shown in Figure S11 and Table S4.

(E) Luciferase activity in the indicated cells transfected with pGL3 containing the indicated luciferase reporters together with pCMV-β-gal and following expression vectors: pSG5L-HA-Rb, pcDNA3-HA-E2F-1, pcDNA3-HA-E2F-3, pBabe-puro-E2F-DB, pSV-Sport-SREBP-1c, pSV-Sport-dominant negative (DN)-SREBP-1c, pBabe-neo-TAg or pBabe-hygro-E1A. Empty vectors were used as control under the same conditions, and results are normalized by β-gal activity. Relative

luciferase activities are shown as the controls set to 1.0. Bars are mean + SE ($n \geq 3$).

(F) Visualization of ^{3}H-farnesylated proteins in AC61 cells prepared as in (D) and treated under the indicated conditions. Coomassie stain is shown as a loading control.

Figure 7. Analysis of human sporadic MTCs.

(A) IHC analysis of sporadic human MTCs. Of 13 cases analyzed, representative cases are shown. Scale bars: 100 μm.

(B) Chi-square analysis (Fisher's exact test) showing the correlation between pRb and N-Ras expression in 13 sporadic human MTCs. *P* value is indicated ($Chi^2 = 9.55$).

Table 1. Pathological diagnosis of thyroids derived from mice with the indicated genotypes. Average age at examination (AE), number of analyzed thyroids (N), histological diagnosis (adenoma: AD or carcinoma: CA), mean diameter of tumors (MD), percentage of CEA, PCNA or Ki-67 positive cells in tumors are indicated ± SE. (--): No data, NA: not analyzed.

Genotype	AE (months)	N	AD	CA	MD (mm)	CEA (%)	PCNA (%)	Ki-67 (%)
Rb$^{+/+}$; *Ink4a*$^{+/+}$	12.0 ± 1.0	5	0	0	--	--	--	--

Rb$^{+/-}$; *Ink4a*$^{+/+}$	9.8 ± 0.4	9	8	0	1.0 ± 0.2	1.4 ± 0.2	5.4 ± 0.4	4.6 ± 1.7
Rb$^{+/+}$; *Ink4a*$^{-/-}$	11.6 ± 0.4	3	0	0	--	--	--	--
Rb$^{+/-}$; *Ink4a*$^{+/-}$	10.0 ± 0.4	6	0	6	3.9 ± 0.2	66.3 ± 2.5	77.3 ± 2.0	74.7 ± 2.4
Rb$^{+/-}$; *Ink4a*$^{-/-}$	10.1 ± 0.3	8	0	8	8.6 ± 0.2	74.2 ± 2.0	84.2 ± 1.0	86.5 ± 1.8
Rb$^{+/-}$; *ARF*$^{+/+}$; *Ink4a*$^{+/+}$	6.2 ± 0.5	8	2	0	0.2 ± 0.1	NA	NA	NA
Rb$^{+/+}$; *ARF*$^{-/-}$; *Ink4a*$^{-/-}$	6.8 ± 0.1	5	0	0	--	--	--	--
Rb$^{+/-}$; *ARF*$^{+/-}$; *Ink4a*$^{+/-}$	7.3 ± 0.2	5	0	5	1.9 ± 0.2	2.5 ± 0.2	78.8 ± 1.5	76.9 ± 2.2
Rb$^{+/-}$; *ARF*$^{-/-}$; *Ink4a*$^{-/-}$	5.6 ± 0.3	6	0	6	3.5 ± 0.3	2.2 ± 0.3	82.4 ± 1.2	84.1 ± 1.6
Rb$^{+/-}$; *ARF*$^{+/+}$	5.4 ± 0.5	6	0	0	--	--	--	--
Rb$^{+/+}$; *ARF*$^{-/-}$	6.5 ± 1.0	6	0	0	--	--	--	--
Rb$^{+/-}$; *ARF*$^{+/-}$	6.5 ± 1.4	2	0	0	--	--	--	--
Rb$^{+/-}$; *ARF*$^{-/-}$	5.2 ± 0.3	5	0	5	1.7 ± 0.1	2.1 ± 0.2	57.8 ± 2.3	55.6 ± 2.2
Rb$^{+/-}$; *Suv39h1*$^{+/+}$	4.8 ± 0.3	6	0	0	--	--	--	--
Rb$^{+/+}$; *Suv39h1*$^{-/-}$	4.8 ± 0	2	0	0	--	--	--	--
Rb$^{+/-}$; *Suv39h1*$^{+/-}$	5.0 ± 0	3	0	0	--	--	--	--
Rb$^{+/-}$; *Suv39h1*$^{-/-}$	4.6 ± 0.2	8	0	8	3.6 ± 0.1	66.8 ± 2.3	81.1 ± 2.1	79.7 ± 2.3

Shamma et al., Figure 1

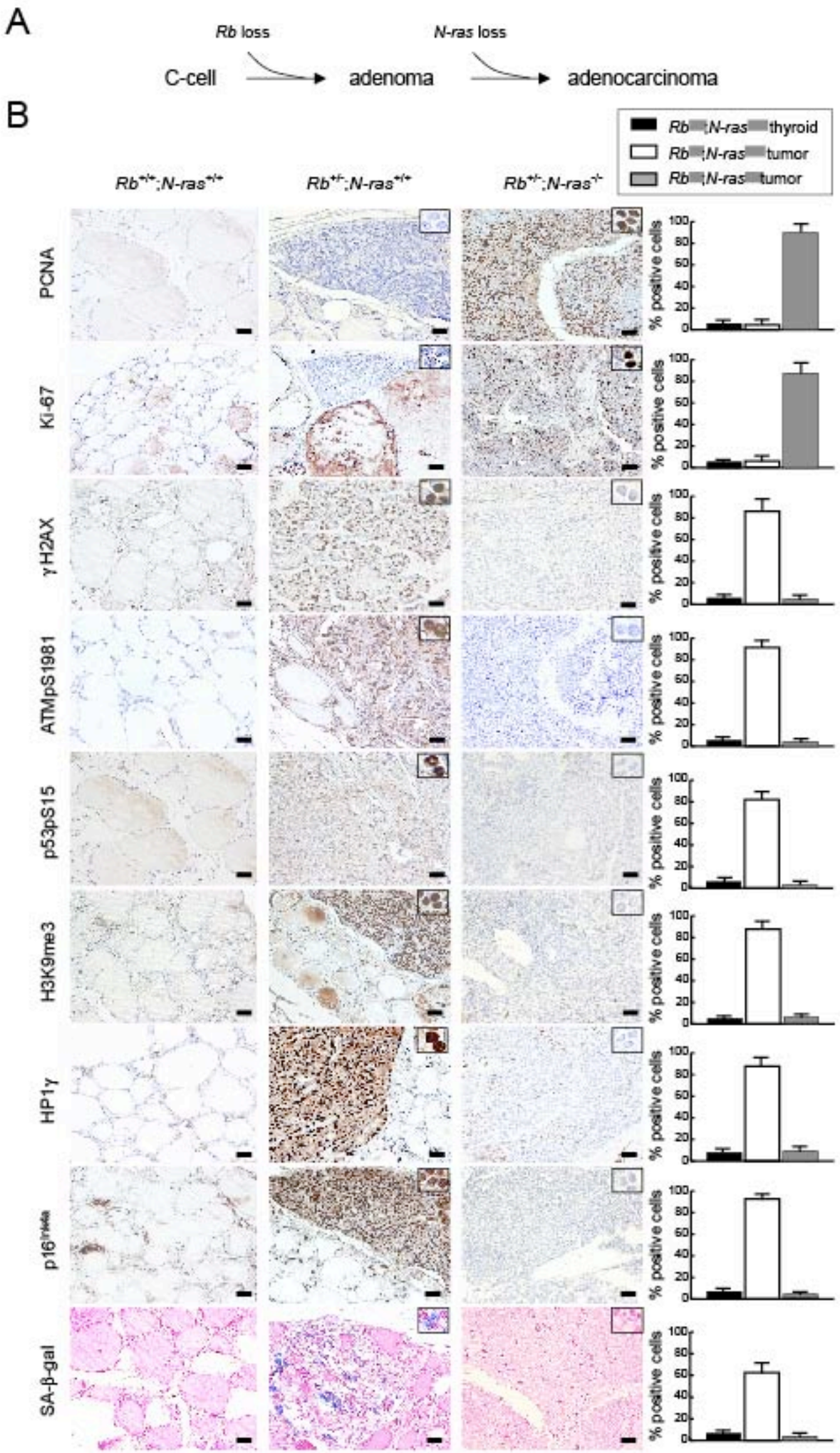

Shamma et al., Figure 2

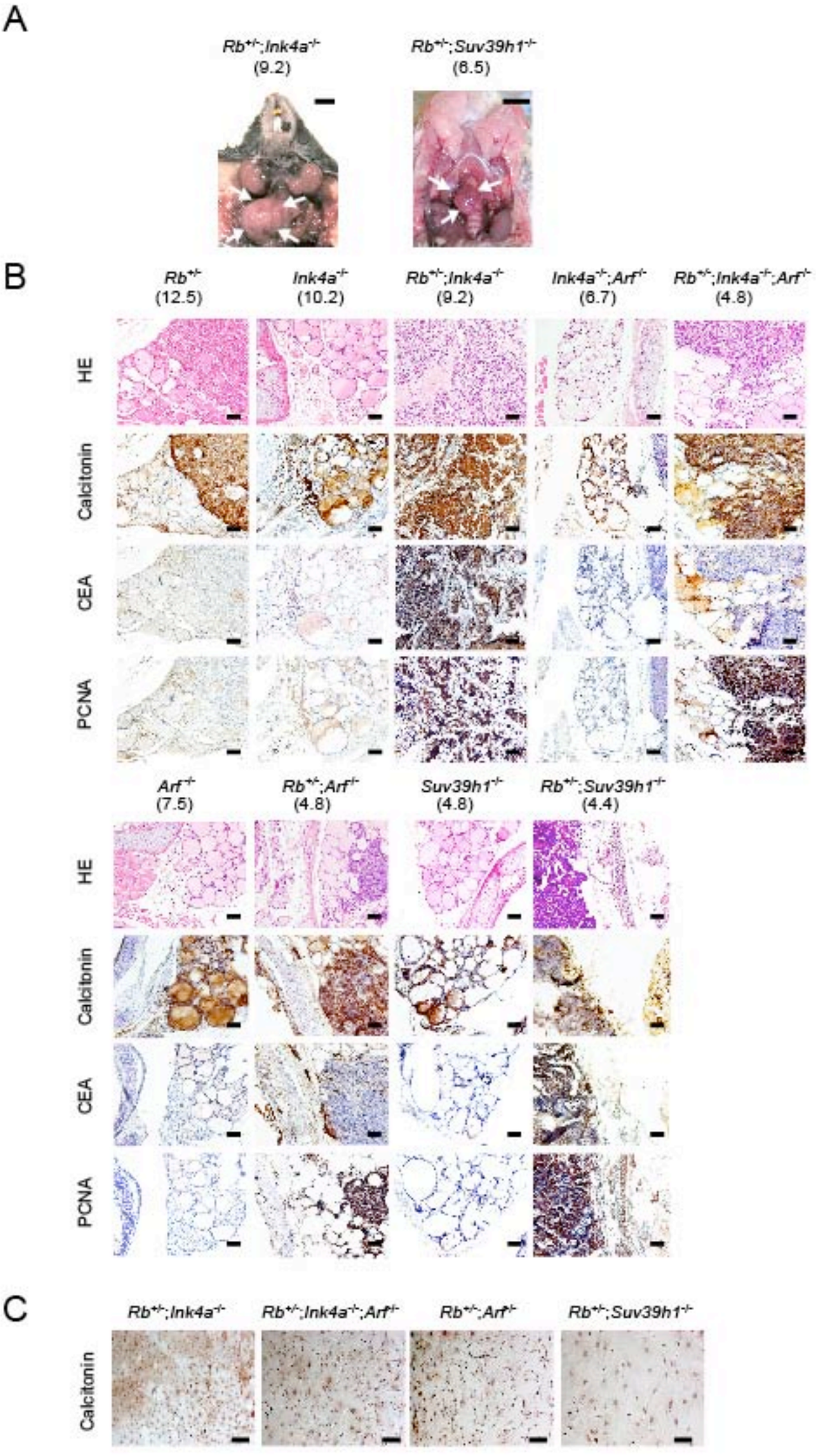

Shamma et al., Figure 3

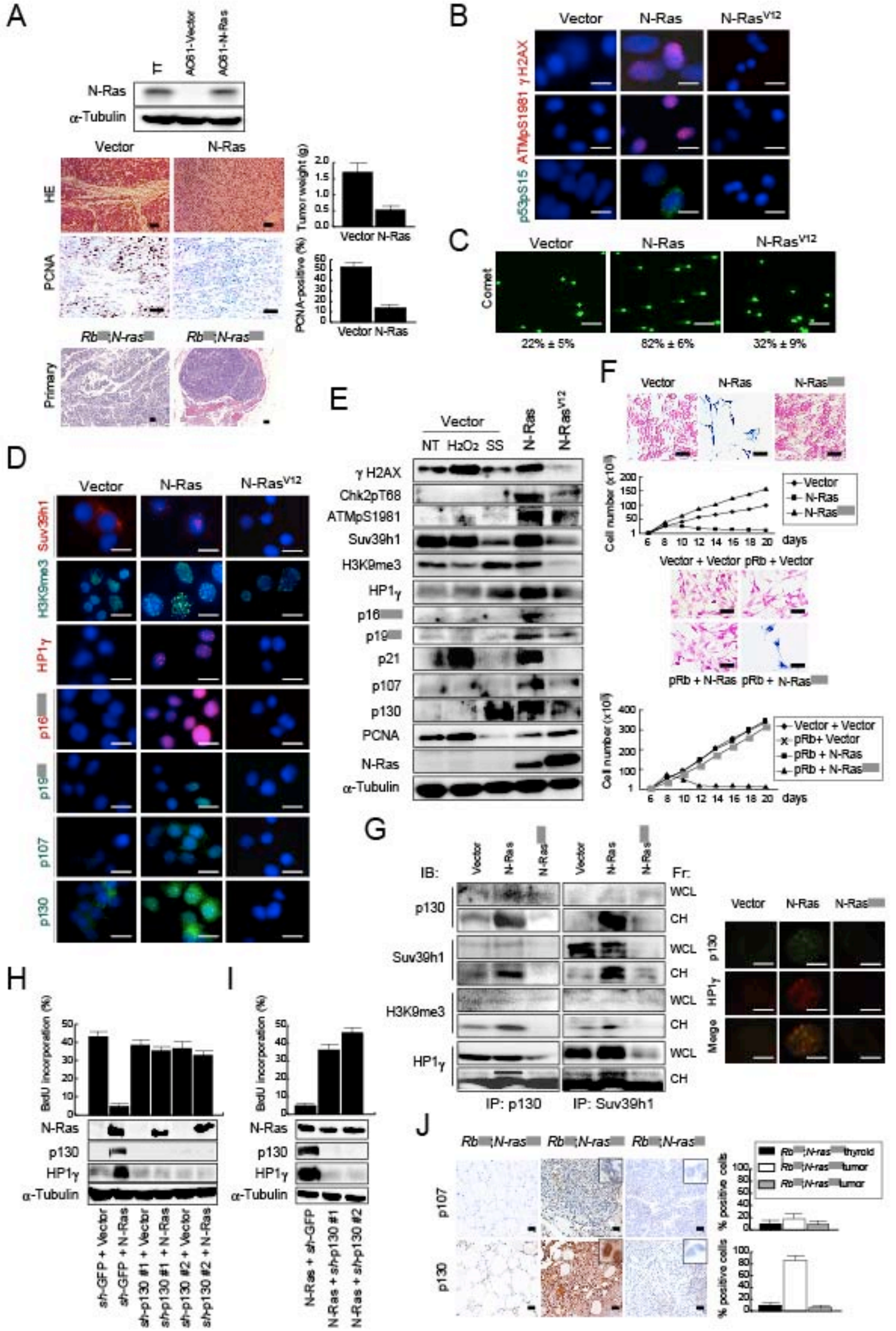

Shamma et al., Figure 4

A

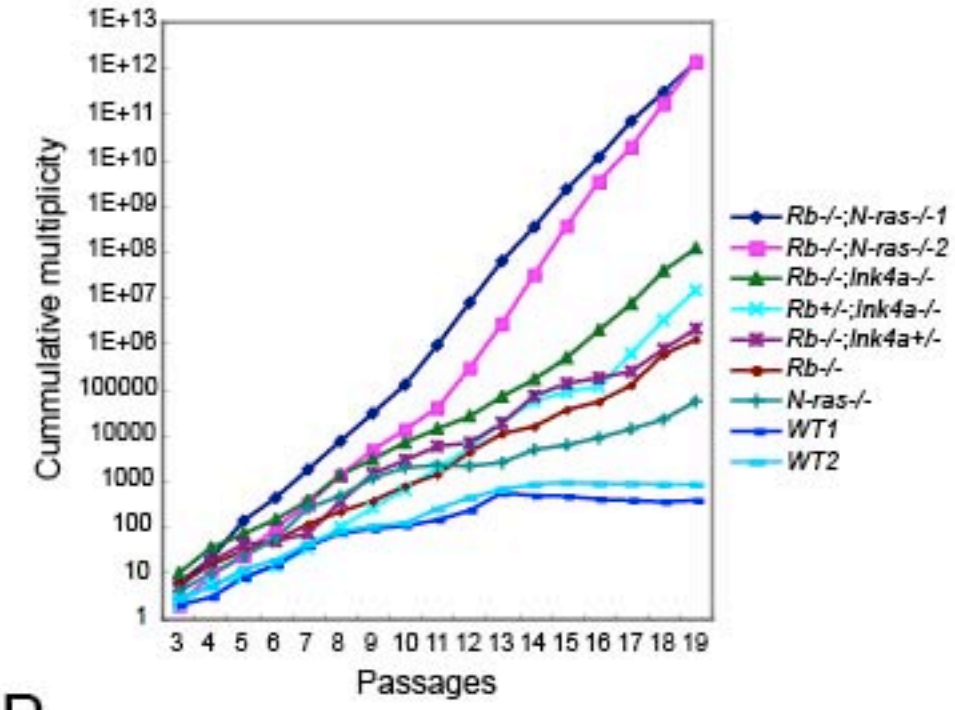

B

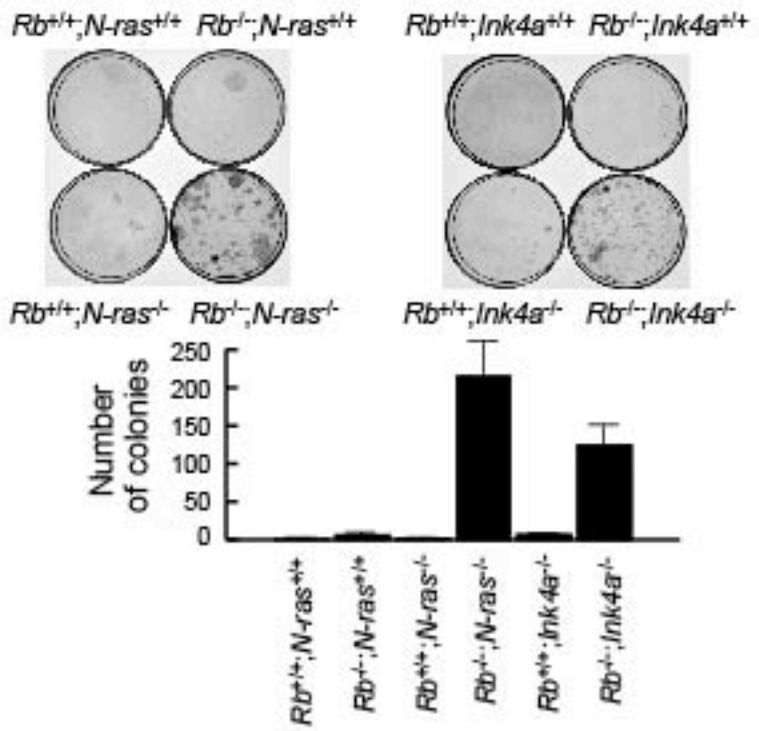

C

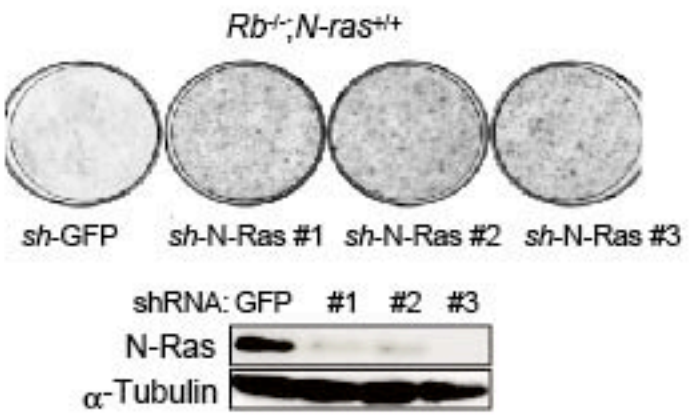

D

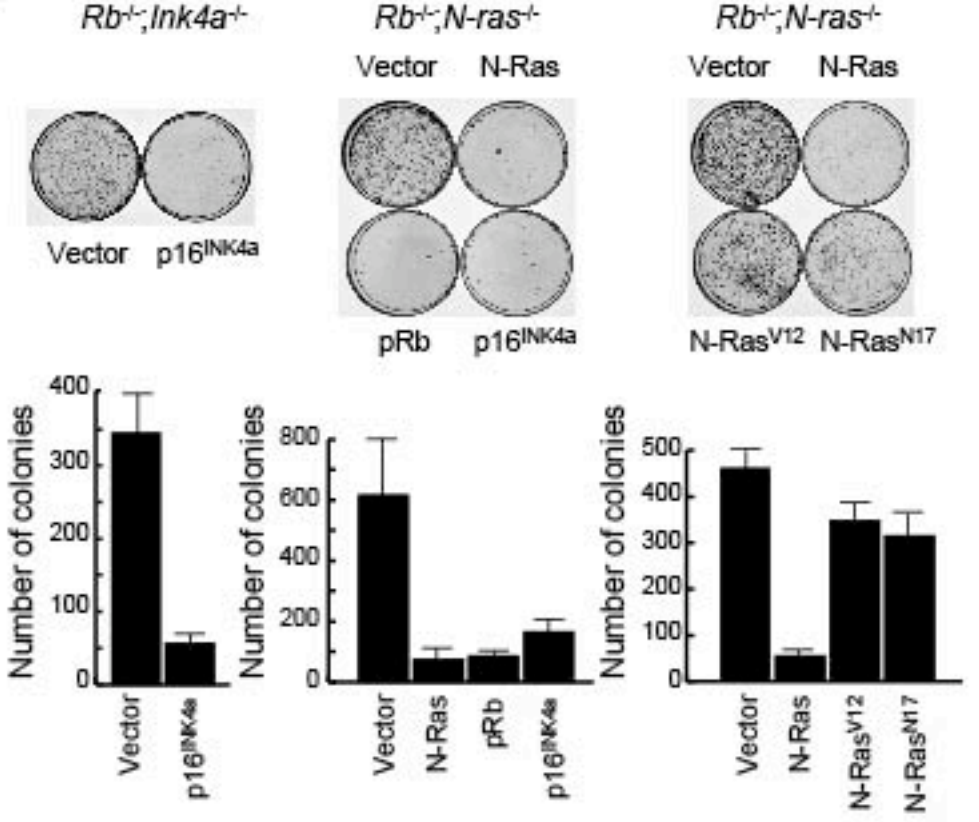

E

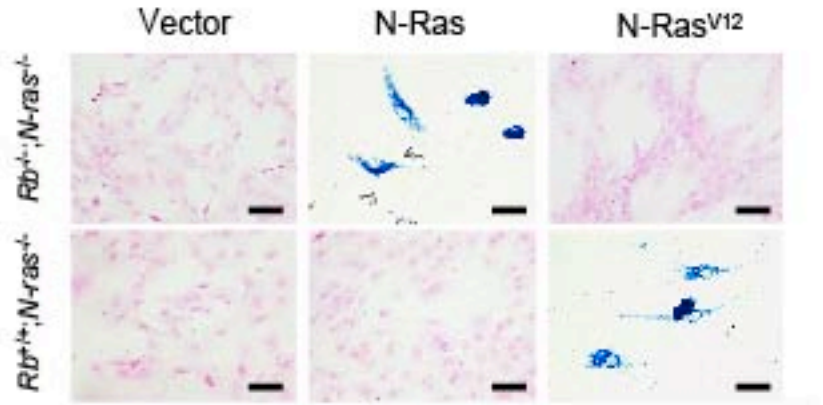

F

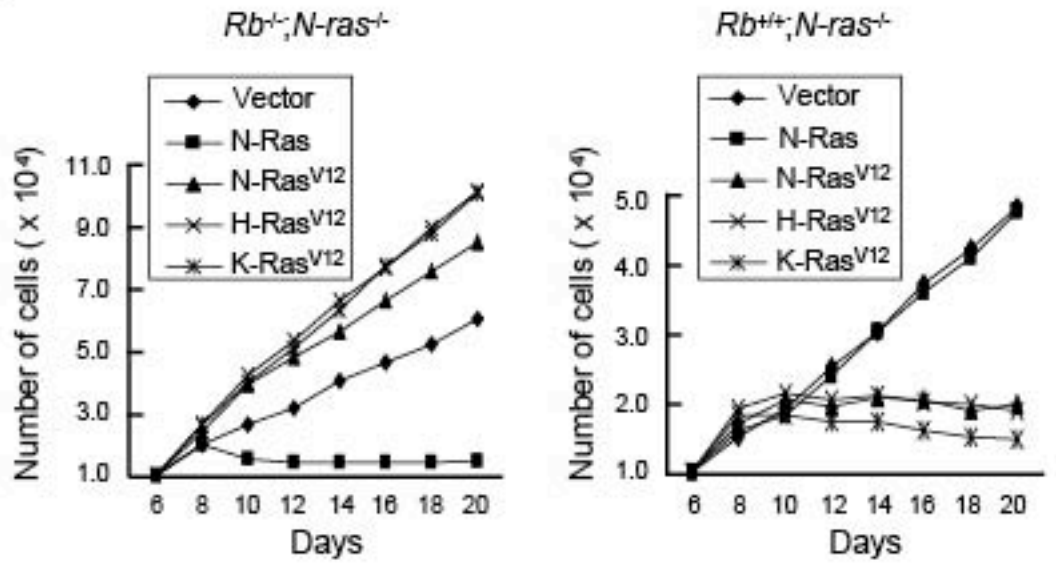

Shamma et al., Figure 5

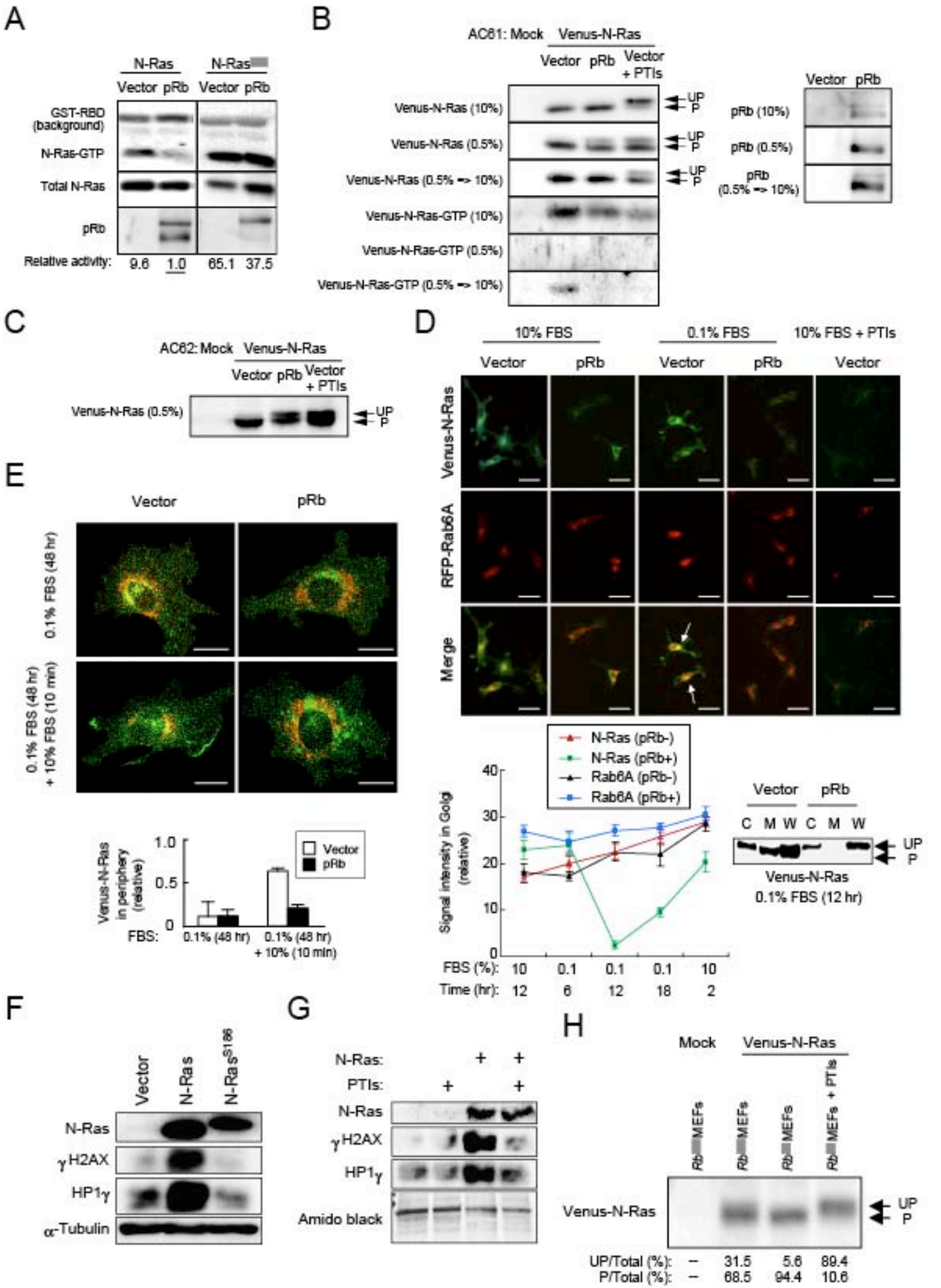

Shamma et al., Figure 6

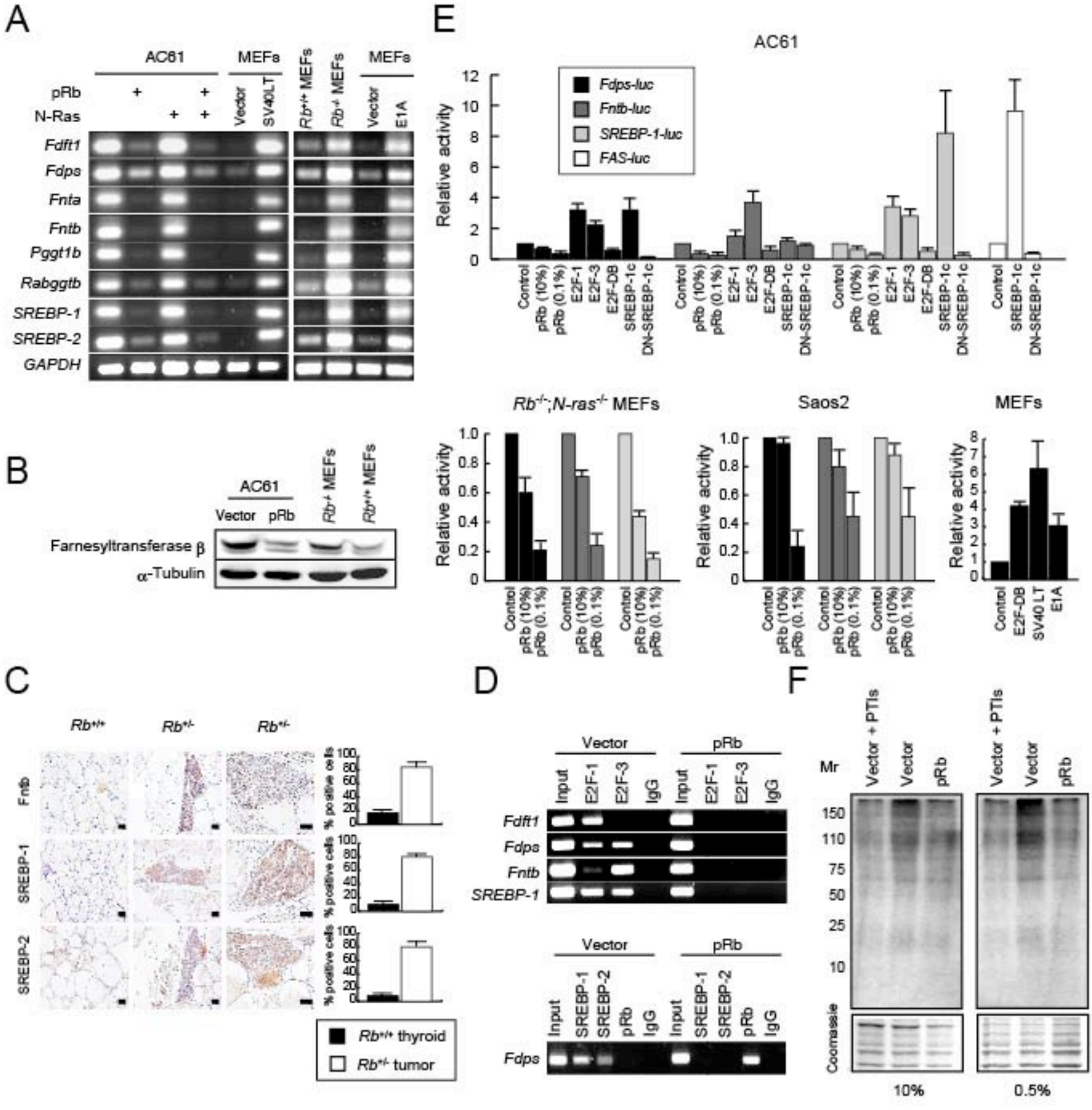

Shamma et al., Figure 7

A

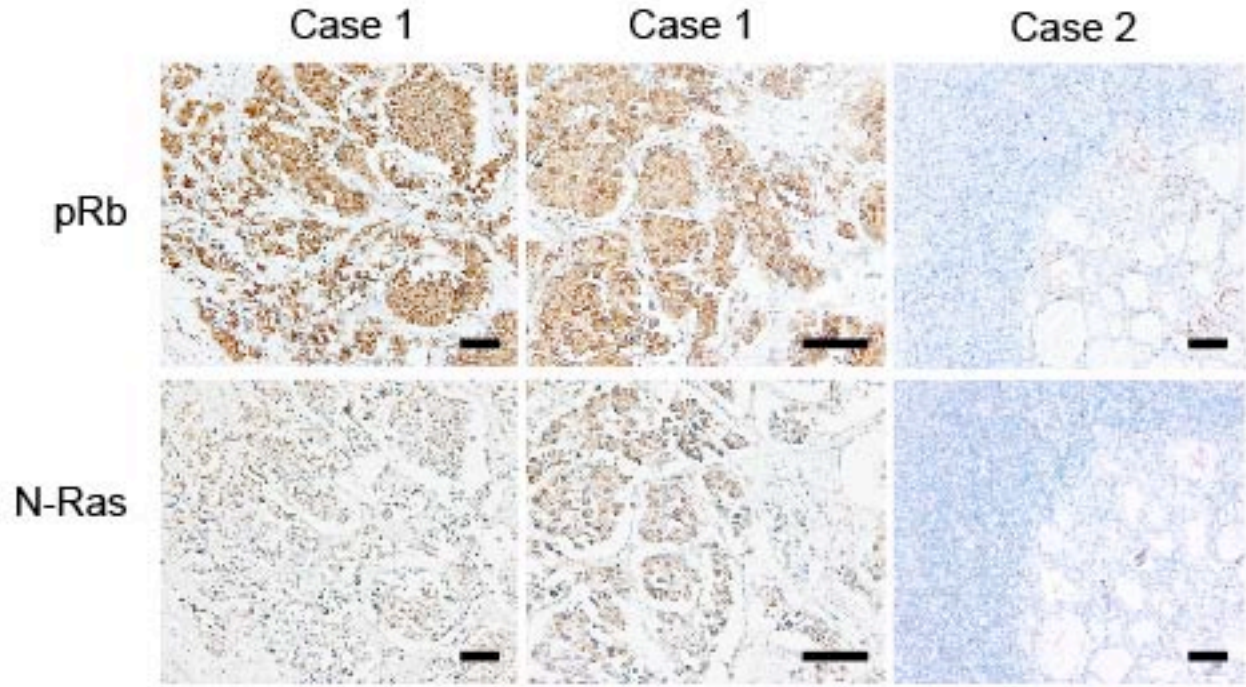

B

	N-Ras	
pRb	Positive	Negative
Positive	6	1
Negative	0	6

p = 0.001998

Cancer Cell, Volume *15*

Supplemental Data

Article

Rb Regulates DNA Damage Response and Cellular Senescence through E2F-Dependent Suppression of N-Ras Isoprenylation

Awad Shamma, Yujiro Takegami, Takao Miki, Shunsuke Kitajima, Makoto Noda, Takao Obara, Takahiro Okamoto, and Chiaki Takahashi

Supplemental Experimental Procedures

Mouse Genotyping

Mouse genotyping was performed as described previsouly (Jacks et al., 1992; Sharpless et al., 2001; Kamijo et al., 1999; Serrano et al., 1996; Peters et al., 2001).

Antibodies

For immunohistochemistry, immunofluorescence or immunoblotting, mouse or rabbit antibodies specific to the following proteins were used: PCNA (SC-7907, Santa-Cruz Biotechnology (SC)), Ki-67 (AB15580, Abcam), γH2AX (05-636, Upstate), ATMpS1981 (200-301-500, Rockland) (for immunohistochemistry only), p53pS15 (PC386, Calbiochem), Trimethyl histone H3 (Lys9) (H3K9me3) (07-442, Upstate), HP1γ (MAB3450, Chemicon), $p16^{INK4a}$ (SC-1661, SC), Calcitonin (SC-20725, SC), CEA (AB33562, Abcam), ATMpS1981 (200-301-400, Rockland), Suv39H1 (AB12405), ARF (AB80, Abcam), p107 (SC-318, SC), p130 (SC-56178, SC), Chk2pT68 (AB38461, Abcam), p21 (556430, BD), N-Ras (OP25, Calbiochem), α-Tubulin (CP06, Calbiochem), pRb (554136, BD), Farnesyltransferase β (SC-4664, SC), Farnesyltransferase α (SC-13964, SC), SREBP-1 (SC-13551, SC) and SREBP-2 (SC-13552, SC). For immunoprecipitation, rabbit antibodies specific to Suv39H1 (SC-25366, SC), p130 (07-282, Upstate) and mouse antibody to pRb (MK-15-3, MBL) were used. For Ras activity and prenylation assay, mouse antibody specific to

N-Ras (OP25, Calbiochem) was used. For ChIP assay, mouse antibodies specific to E2F-1 (SC-193, SC), E2F-3 (SC-878, SC), pRb (MK-15-3, MBL), SREBP-1 (SC-13551, SC) and SREBP-2 (SC-13552, SC) were used.

Immunohistochemistry

Paraffin embedded mouse C cell tumors or human MTCs were deparaffinized, rehydrated and unmasked in 0.25 mM EDTA at 95^{o}C for 50 min. Tissue sections were immunostained using Dako Envision kit (K1390) and counterstained with hematoxylin.

Retroviruses and Plasmids

pBabe-puro-N-ras, N-ras^{V12}, N-ras^{N17}, H-ras^{V12} were made by subcloning cDNAs from pLenti6/V5 vectors previously described (Takahashi et al., 2006). pBabe-puro-N-ras^{SAAX} (N-ras^{S186}) was generated by introducing a Cysteine to Serine mutation into N-Ras by using PCR with mutated oligoncletide. pBabe-puro-p16^{INK4a} (Alevizopoulos et al., 1997), pBabe-puro-E2F-DB (Rowland et al., 2002), pBabe-neo-TAg (Hahn et al., 2002), pCMV-pRb (Qin et al., 1992) and pCMV-β-gal (Takahashi et al., 2003) were described previously. pLXSB-Rb was made by subcloning the cDNA from pSG5-Rb (Shirodkar et al., 1992). pGL3-Fdps-luc (position, –1601~-1 from the predicted transcription initiation site), pGL3-Fntβ-luc (position, -2141~+267) and pGL3–SREBP-1-luc (position, -2161~+872) were made by subcloning C57BL/6 mouse genomic DNAs amplified by PCR. pSV-Sport-SREBP-1c, its dominat negative mutant (Tontonoz et al., 1993) and pGL3-FAS-luc (Kim et al., 1998) were purchased from Addgene (Boston, MA) with the permission from B. Spiegelman. pCXN2-RFP-Rab6A was a gift from T. Taguchi, pCAGGS-Venus^{A207R}-N-Ras (A207R stands for an Alanine to Arginine mutation intruoduced into Venus protein in an aim to make it monomeric) from M. Matsuda, and pcDNA3-HA-E2F-1 and pcDNA3-HA-E2F-3 from S. Gaubatz. For retrovirus production, EcoPak2 (Clontech) cells were used. Retrovirus expressing K-Ras^{V12} (pMIKcys) was a gift from M. Noda. Transfection of C cell tumor cell lines and MEFs was done using FuGene6 (Roche). AC61 cells or MEFs transduced with pBabe-puro or pLXSB vectors were slected with 4 μg/ml puromycin or 8 μg/ml blasticidin S respectively for 36~48 hr.

Immunofluorescence

Texas red-conjugated goat anti-mouse or Alexa Fluor-conjugated 488 goat anti-rabbit antibody (T862 and A11034 respectively, Molecular Probes) was used as the secondary antibody. DNA was

visualized by 4', 6-diamino-2-phenylindole (DAPI).

Senescence-Associated β-Galactosidase Assays

SA-β-gal assay was performed in vitro as described previously (Dimri et al., 1995). For *in situ* assay, tissues were fixed in 4% paraformaldehyde (PFA) in phosphate buffered saline (PBS) for 12 hr at 4C^{o}, incubated in 70% ethanol for 24 hr at 4^{o}C, and embedded in paraffin. Four μm sections were prepared on lysine-coated glass slides, deparaffinized, rehydrated, and unmasked with 0.25 mM EDTA for 50 minutes at 95 ^{o}C. Tissue sections were stained in 40 mM Citric acid, 40 mM NaPO4, 5 mM K4[Fe(CN)6], 5 mM K3[Fe(CN)6], 150 mM NaCl, 2 mM MgCl2, 0.02% NP-40 (pH 6.0) with 1 mg/ml 5-bromo-4-chloro-3-indolyl-β-D-galactoside (X-gal) for 16 hr at 37 ^{o}C.

Immunoblotting

Whole cell lysates were prepared in buffer (Miki et al., 2007) or in acid-extraction buffer (Fischle et al. 2005) as described previously.

Cell Fractionation

Cell fractionation was performed as described previously (Amin et al. 2003).

Immunoprecipitation

Whole cell lysates or chomatin fraction was extracted as described previously (Miki et al., 2007; Fischle et al., 2005) and immunoreacted with specific antibodies.

Telomerase Detection

Cells were infected with pBabe-puro or pBabe-puro-N-ras, selected with 4 μg/ml puromycin for 2 days, and analyzed either by TRAP assay or immunoblotting 11 days after the initial infection. TRAP assay was performed using TRAPEZE telomerase detection kit from Chemicon (S7700) according to the manufacturer's protocol. The mTERT immunoblotting was performed using anti-telomerase specific antibody from Calbiochem (582000) as described previously (Kharbanda et al., 2000).

FLAG-Tagged N-Ras

pBabe-puro-N-ras was used as a template for PCR using sense

5'-GAGGAATTCATGGATTACAAAGATGACGATGACAAAACTGAGTACAAACTGGTGGTGGTT-3' and antisense 5'-GACGGGATCCTTACATCACCACACATGGCA-3' primers to generate a FLAG-tag fused to the N-terminal end of N-Ras. Amplified DNA was inserted into pLXSB (Miki et al., 2007).

3D Imaging

Ten two-dimensional (2D) slices at 1 μm thickness each taken by confocal laser fluorescence microscope (Fluoroview; Olympus) were assembled to generate thee-dimensional (3D) images using FV300 image analysis program (Olympus).

Microarray

1.0 x10^6 AC61 cells were infected with titer known retrovirus derived from pLXSB or pLXSB-Rb, and selected with 8 μg/ml blasticidin S for 36 hr. Resultant cells were grown for 48 hr without blasticidin S in 10% FBS, harvested on ice, and quickly frozen. RNA was extracted and analyzed by using Genechip mouse 430.2 (Affymetrix) and DNA MicroArray viewer (KURABO, Japan) at the microarray core facility of KURABO Co. (Neyagawa, Osaka, Japan).

Promoter Analysis

2 kb upstream and 1 kb downstream of the predicted transcription initiation site of genes in genomic DNA sequences were retrieved from the mouse genome informatics (MGI) data base or from human genome database provided by GenBank. The sequences were searched for the sterol responsive element (SRE) at http://motif.genome.jp/ and E2F binding consensus sequences at http://compel.bionet.nsc.ru/FunSite/SiteScan.html as previously reported (Nahle et al. 2003). Accession numbers of genome sequences containing each gene are as following: *Fdft1*, 102706 for mouse and NC_000008 for human; *Fdps*, 104888 and NC_000001; *Fnta*, 104683 and NC_000008; *Fntb*, 1861305 and NC_000014; *Pggt1b*, 1917514 and NC_000005; *Rabggtb*, 99537 and NC_000001; *SREBP-1*, 107606 and NC_000017, and *SREBP-2*, 107585 and NC_000022.

ChIP Assay of Fdps Promoter in AC61 Cells Transfected with pRb Mutants

2.5 μg of pSG5L-HA-pRb$^{\Delta ex22}$ or pSG5L-HA-pRb$^{\Delta ex4}$ (Sellers et al., 1998) were introduced into AC61 cells together with 0.25 μg pLSXB, and selected with 8 μg/ml blatsticidin S. Resultant cells were analyzed by ChIP assay using the same antibodies and primers as used in Figure 6D (lower

panel). Position and sequence of these primers in *Fdps* gene promoters are indicated in Figure S11 and Table S4 (*Fdps**).

Luciferase Assay

5.0 x 10^3 AC61 or 1.0 x 10^4 *Rb*$^{-/-}$;*N-ras*$^{-/-}$ MEFs, Saos2 cells or wild-type MEFs were transfected with 0.125 μg of luciferase reporter constructs and 0.125 μg pCMV-β-gal together with 0.25 ~1.25 μg expression vectors. Luciferase activity and β-gal activity in cells was measured 48~72 hr after transfection as described previously (Takahashi et al., 2003). β-gal activity was used to normalize the luciferase activity in each transfection.

Supplemental References

Alevizopoulos, K., Vlach, J., Hennecke, S., and Amati, B. (1997). Cyclin E and c-Myc promote cell proliferation in the presence of p16INK4a and of hypophosphorylated retinoblastoma family proteins. Embo J 16, 5322-5333.

Amin, R. H., Chen, H. Q., Veluthakal, R., Silver, R. B., Li, J., Li, G., and Kowluru, A. (2003). Mastoparan-induced insulin secretion from insulin-secreting betaTC3 and INS-1 cells: evidence for its regulation by Rho subfamily of G proteins. Endocrinology 144, 4508-4518.

Dimri, G. P., Lee, X., Basile, G., Acosta, M., Scott, G., Roskelley, C., Medrano, E. E., Linskens, M., Rubelj, I., Pereira-Smith, O., and et al. (1995). A biomarker that identifies senescent human cells in culture and in aging skin in vivo. Proc Natl Acad Sci U S A 92, 9363-9367.

Fischle, W., Tseng, B. S., Dormann, H. L., Ueberheide, B. M., Garcia, B. A., Shabanowitz, J., Hunt, D. F., Funabiki, H., and Allis, C. D. (2005). Regulation of HP1-chomatin binding by histone H3 methylation and phosphorylation. Nature 438, 1116-1122.

Hahn, W. C., Dessain, S. K., Brooks, M. W., King, J. E., Elenbaas, B., Sabatini, D. M., DeCaprio, J. A., and Weinberg, R. A. (2002). Enumeration of the simian virus 40 early region elements necessary for human cell transformation. Mol Cell Biol 22, 2111-2123.

Jacks, T., Fazeli, A., Schmitt, E. M., Bronson, R. T., Goodell, M. A., and Weinberg, R. A. (1992). Effects of an Rb mutation in the mouse. Nature 359, 295-300.

Kamijo, T., Bodner, S., van de Kamp, E., Randle, D. H., and Sherr, C. J. (1999). Tumor spectrum in ARF-deficient mice. Cancer Res 59, 2217-2222.

Kharbanda, S., Kumar, V., Dhar, S., Pandey, P., Chen, C., Majumder, P., Yuan, Z. M., Whang, Y., Strauss, W., Pandita, T. K., et al. (2000). Regulation of the hTERT telomerase catalytic subunit by the c-Abl tyrosine kinase. Curr Biol 10, 568-575.

Kim, J. B., Wright, H. M., Wright, M., and Spiegelman, B. M. (1998). ADD1/SREBP1 activates PPARgamma though the production of endogenous ligand. Proc Natl Acad Sci U S A 95, 4333-4337.

Miki, T., Takegami, Y., Okawa, K., Muraguchi, T., Noda, M., and Takahashi, C. (2007). The reversion-inducing cysteine-rich protein with Kazal motifs (RECK) interacts with membrane type 1 matrix metalloproteinase and CD13/aminopeptidase N and modulates their endocytic pathways. J Biol Chem 282, 12341-12352.

Nahle, Z., Polakoff, J., Davuluri, R. V., McCurrach, M. E., Jacobson, M. D., Narita, M., Zhang, M. Q., Lazebnik, Y., Bar-Sagi, D., and Lowe, S. W. (2002). Direct coupling of the cell cycle and cell death machinery by E2F. Nat Cell Biol 4, 859-864.

Peters, A. H., O'Carroll, D., Scherthan, H., Mechtler, K., Sauer, S., Schofer, C., Weipoltshammer, K., Pagani, M., Lachner, M., Kohlmaier, A., et al. (2001). Loss of the Suv39h histone methyltransferases impairs mammalian heterochomatin and genome stability. Cell 107, 323-337.

Qin, X. Q., Chittenden, T., Livingston, D. M., and Kaelin, W. G., Jr. (1992). Identification of a growth suppression domain within the retinoblastoma gene product. Genes Dev 6, 953-964.

Rowland, B. D., Denissov, S. G., Douma, S., Stunnenberg, H. G., Bernards, R., and Peeper, D. S. (2002). E2F transcriptional repressor complexes are critical downstream targets of p19(ARF)/p53-induced proliferative arrest. Cancer Cell 2, 55-65.

Sellers, W. R., Novitch, B. G., Miyake, S., Heith, A., Otterson, G. A., Kaye, F. J., Lassar, A. B., and Kaelin, W. G., Jr. (1998). Stable binding to E2F is not required for the retinoblastoma protein to activate transcription, promote differentiation, and suppress tumor cell growth. Genes Dev 12, 95-106.

Serrano, M., Lee, H., Chin, L., Cordon-Cardo, C., Beach, D., and DePinho, R. A. (1996). Role of the INK4a locus in tumor suppression and cell mortality. Cell 85, 27-37.

Sharpless, N. E., Bardeesy, N., Lee, K. H., Carrasco, D., Castrillon, D. H., Aguirre, A. J., Wu, E. A., Horner, J. W., and DePinho, R. A. (2001). Loss of p16Ink4a withetention of p19Arf predisposes mice to tumorigenesis. Nature 413, 86-91.

Shirodkar, S., Ewen, M., DeCaprio, J. A., Morgan, J., Livingston, D. M., and Chittenden, T. (1992). The transcription factor E2F interacts with the retinoblastoma product and a p107-cyclin A complex in a cell cycle-regulated manner. Cell 68, 157-166.

Takahashi, C., Contreras, B., Iwanaga, T., Takegami, Y., Bakker, A., Bronson, R. T., Noda, M., Loda, M., Hunt, J. L., and Ewen, M. E. (2006). Nras loss induces metastatic conversion of Rb1-deficient neuroendocrine thyroid tumor. Nat Genet 38, 118-123.

Tontonoz, P., Kim, J. B., Graves, R. A., and Spiegelman, B. M. (1993). ADD1: a novel helix-loop-helix transcription factor associated with adipocyte determination and differentiation. Mol Cell Biol 13, 4753-4759.

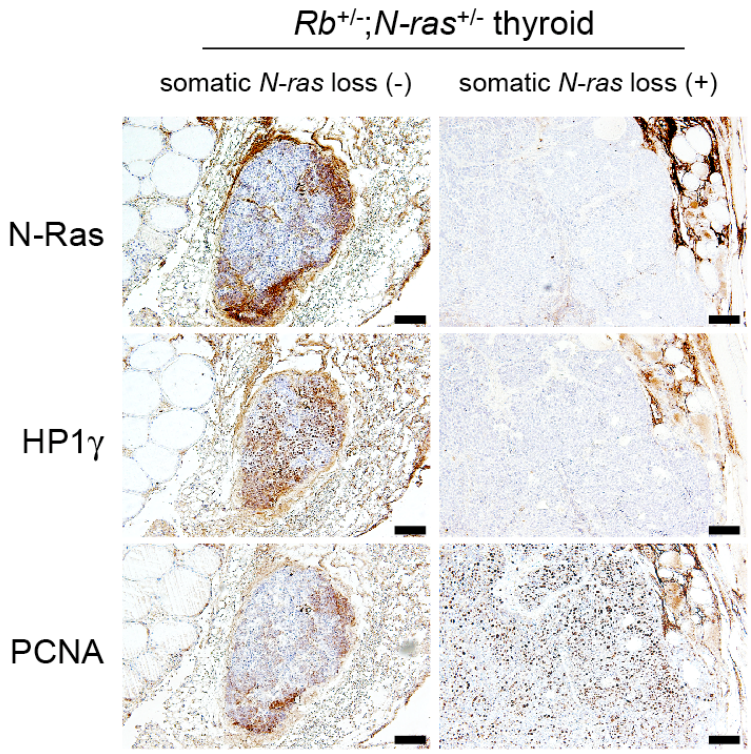

Figure S1. Analysis of *Rb*-Deficient C Cell Tumors that Acquired Somatic Loss of *N-ras*

Immunohistochemical analysis of the serial sections of C cell tumors developed in $Rb^{+/-}$;$N\text{-}ras^{+/-}$ mice that have not (-) or have acquired (+) somatic loss of wild-type *N-ras* allele following *Rb*-loss. Antibodies specific to the indicated proteins were used. Scale bars = 100 μm.

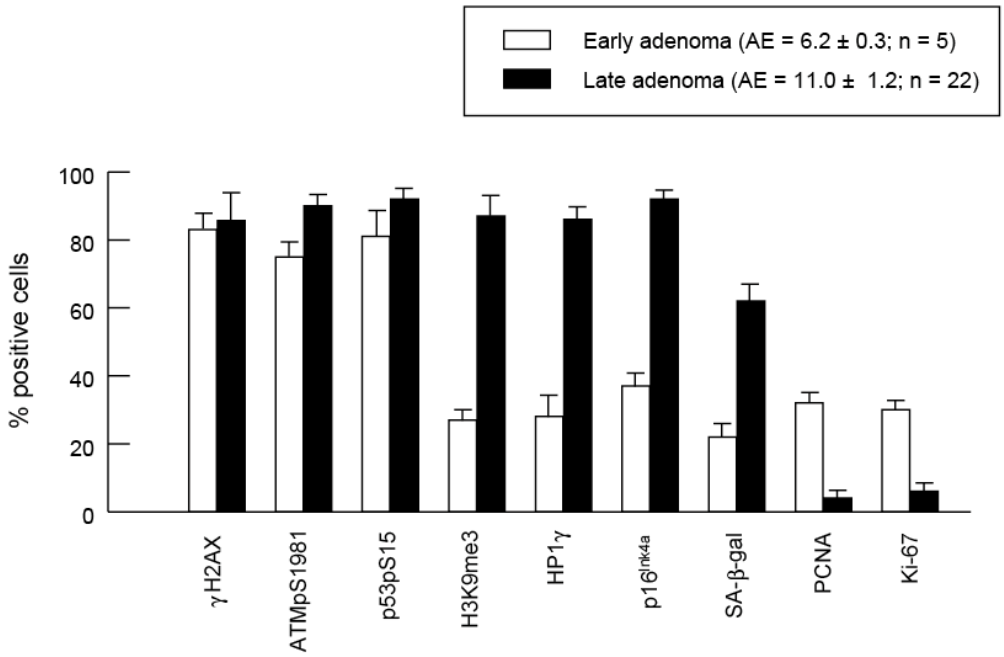

Figure S2. Frequency of DDR and Cellular Senescence Markers in *Rb*-Deficient C Cell Early Adenomas and Late Adenomas

Thyroid glands of the indicated age of $Rb^{+/-}$ mice were analyzed. Tumors were stained with antibodies specific to the indicated proteins. Frequency of positive cells in immunohistochemical analysis was quantified. Bars are mean + SE.

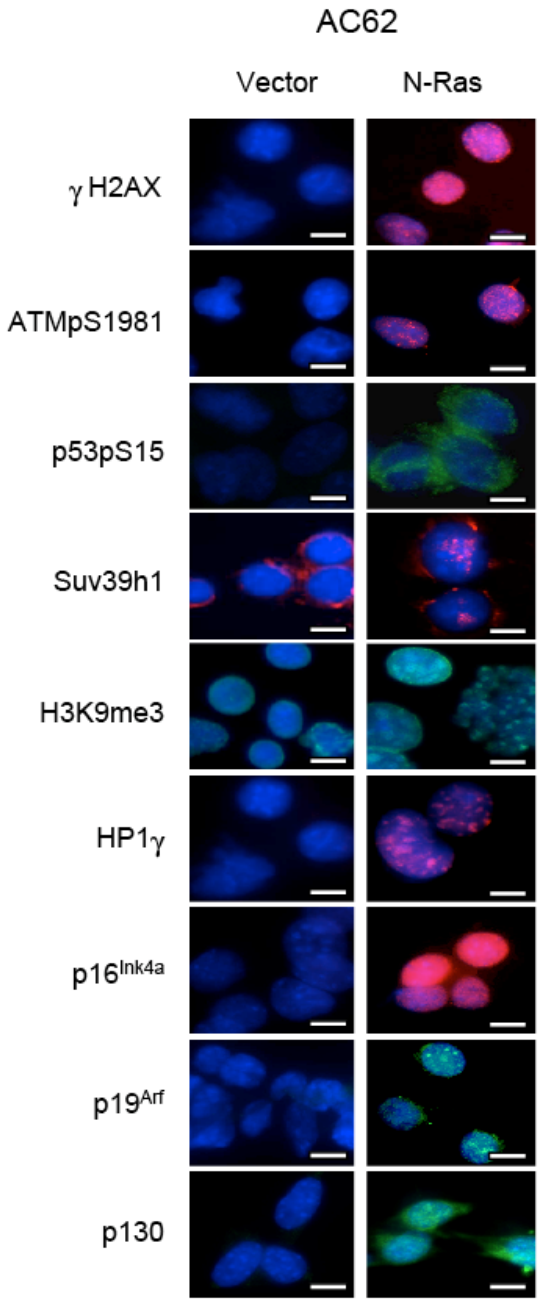

Figure S3. N-Ras Induced DDR and Cellular Senescence in Other *Rb*-Deficient *N-ras*$^{-/-}$ C Cell Adenocarcinoma Cell Lines Similar to AC61

AC62, one of other cell lines independently prepared from C cell tumor developed in an *Rb*$^{+/-}$;*N-ras*$^{-/-}$ mouse, was examined as in Figure 3B and D. Scale bars = 10 μm.

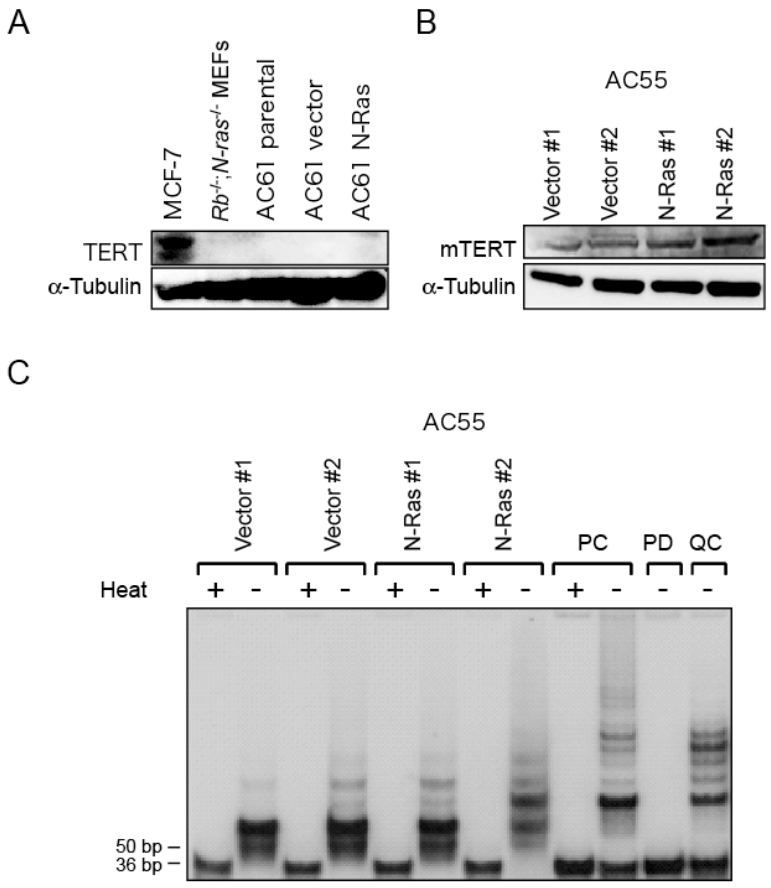

Figure S4. Effect of N-Ras on Telomerase Activity in *Rb*-Deficient Cells

(A) MCF-7 cells, *Rb*$^{-/-}$;*N-ras*$^{-/-}$ MEFs and AC61 cells (parental and those infected with pBabe-puro or pBabe-puro-N-ras) were analyzed for TERT expression by immunoblotting.

(B) Immunoblot analysis of mTERT expression levels in another C cell adenocarcinoma cell line (AC55) infected with pBabe-puro or pBabe-puro-N-ras, selected and cultured for 7 days. #1 and #2 were independently established.

(C) The telomeric repeat amplification protocol (TRAP) assay of cells analyzed in panel (B). Heat inactivation was performed to suppress telomerase activity. 36 base pair bands are internal control.

PC: positive control, PD: primer dimmer and QC: quantitative control.

A

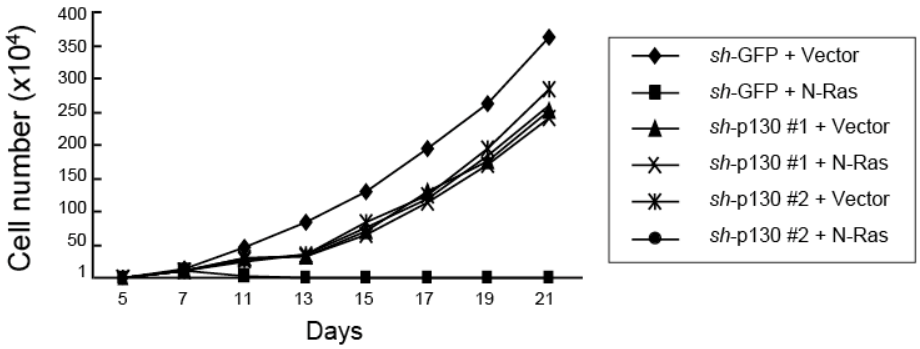

B

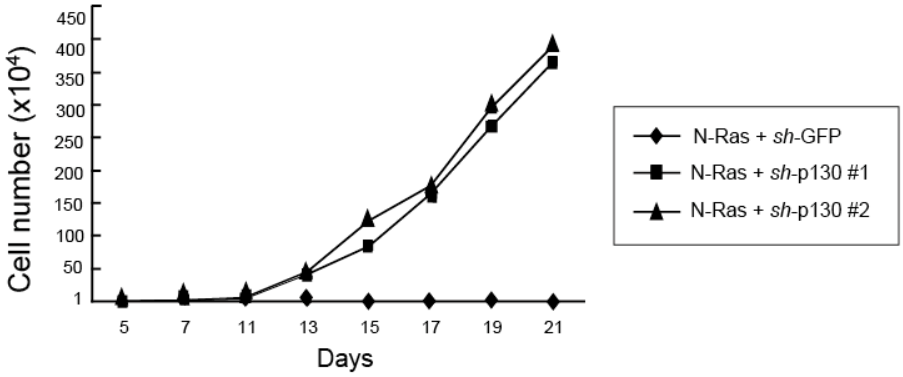

Figure S5. Proliferation of AC61 Cells Transduced with N-Ras and shRNA Targeting p130

(A) AC61 cells were infected with lentivirus expressing the indicated shRNAs, and selected with puromycin. After 5 days from the initial infection, resultant cells were infected with pLXSB or pLXSB-N-ras, selected with blasticidin S, and analyzed. Growth curve from day 5 onwards after the last infection is shown.

(B) AC61 cells were infected with pLXSB or pLXSB-N-ras, and selected with blasticidin S. After 14 days from the initial infection, resutant cells were infected with lentivirus expressing the indicated shRNAs, selected with puromycin, and analyzed. Growth curve from day 5 onwards after the last infection is shown.

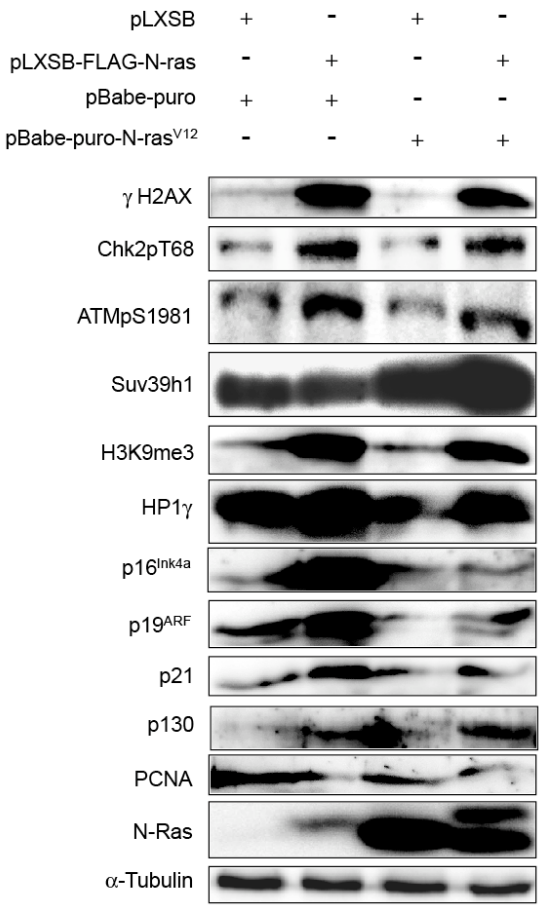

Figure S6. Differential Functions of N-Ras and N-Ras^{V12} in Inducing DDR and Cellular Senescence in *Rb*$^{-/-}$;*N-ras*$^{-/-}$ MEFs

Rb$^{-/-}$;*N-ras*$^{-/-}$ MEFs were simultaneously infected with retroviruses derived from the indicated plasmids, and selected with blasticidin S and puromycin. Resultant cells were cultured for 12 days, and analyzed by immunoblotting. Antibodies specific to the indicated proteins were used.

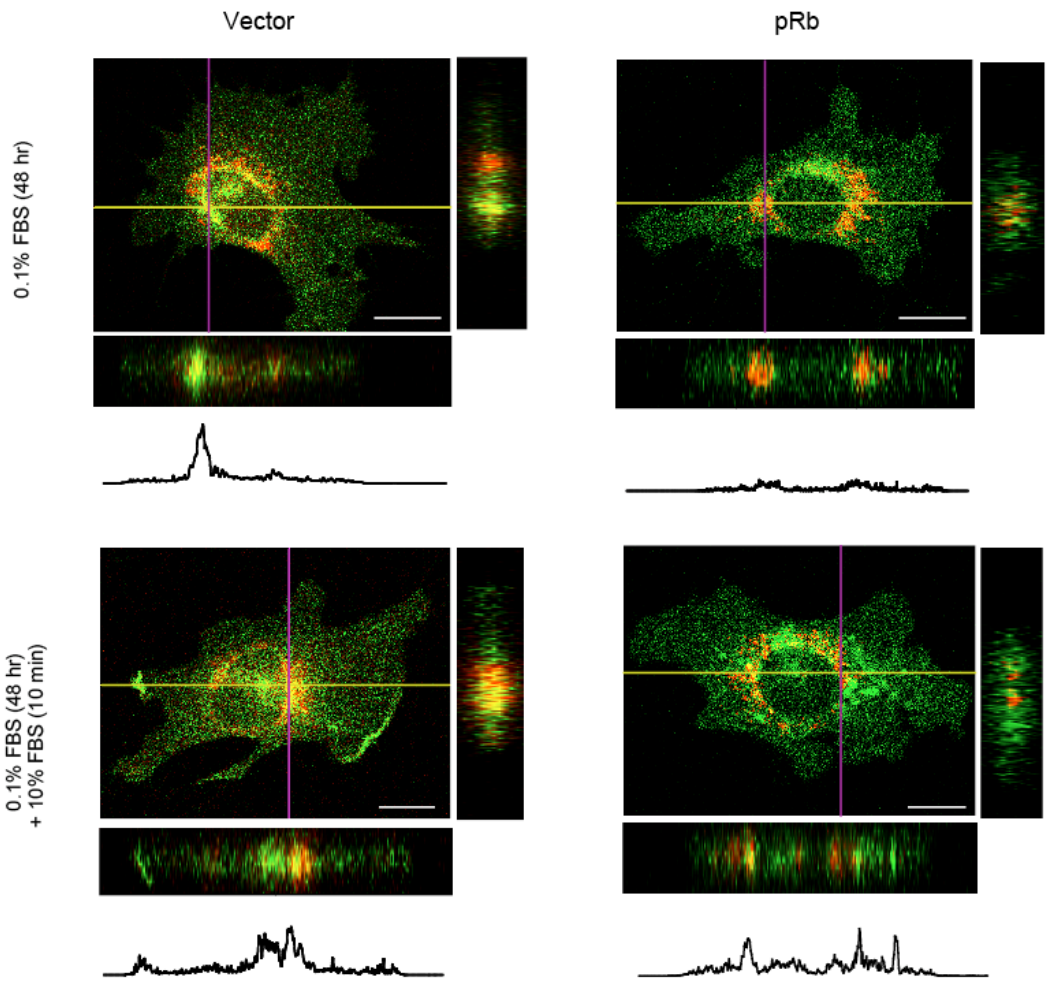

Figure S7. 3D Imaging of Venus-N-Ras and RFP-Rab6A in AC61 Cells in the Absence or Presence of pRb

Cells analyzed in Figure 5D were further analyzed at the indicated levels by the 3D method. Scale bars = 10 μm. Intensity of green signals in the 3D image at the level indicated by yellow line is measured using NIH ImageJ 1.4 program.

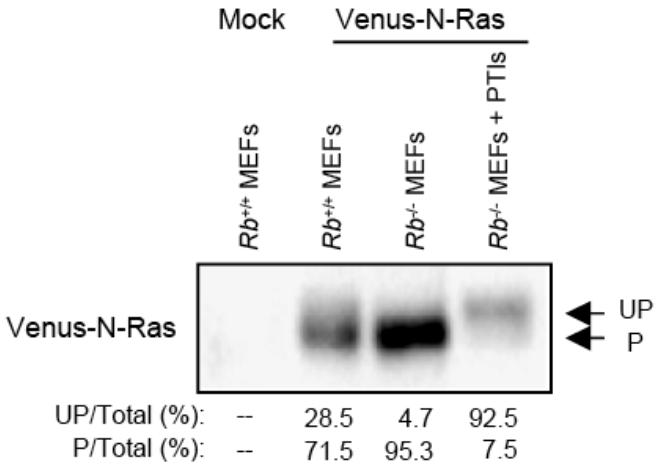

Figure S8. Accelerated N-Ras Isoprenylation in *Rb*-Deficient MEFs

Another pair of MEFs was examined as in Figure 5H.

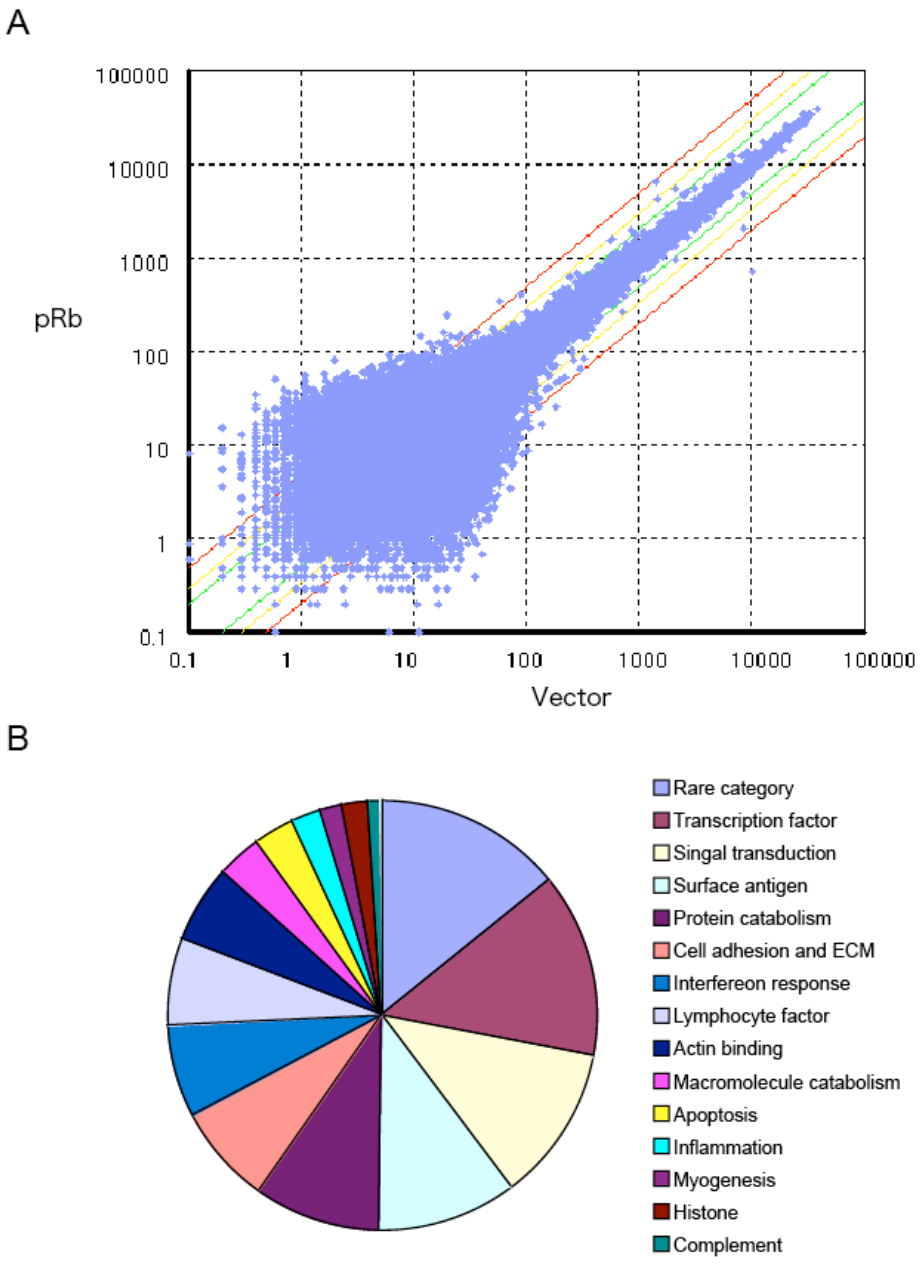

Figure S9. Microarray Analysis of AC61 Cells Reconstituted with pRb

(A) Dot blot presentation of the microarray analysis comparing gene expression profiles in pLSXB and pLXSB-Rb-infected AC61 cells. RNA was extracted at 72 hr after viral infection. X-axis represents expression level in pLSXB, and Y-axis in pLXSB-Rb infected cells.

(B) Simplified ontology of 396 significantly upregulated genes with p value < 0.001 determined by Wilcoxon's Signed Rank test.

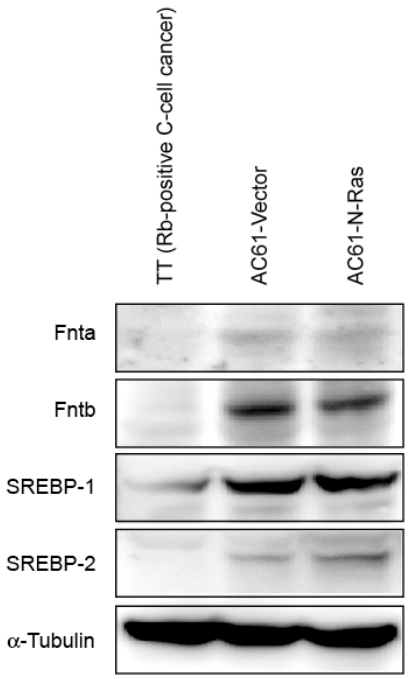

Figure S10. Correlation of the pRb Status and the Expression of Proteins Involved in Protein Isoprenylation

TT cells (pRb-positive human C cell cancer line) and AC61 cells infected with pBabe-puro (vector) or pBabe-puro-N-ras were analyzed by IB for the indicated proteins.

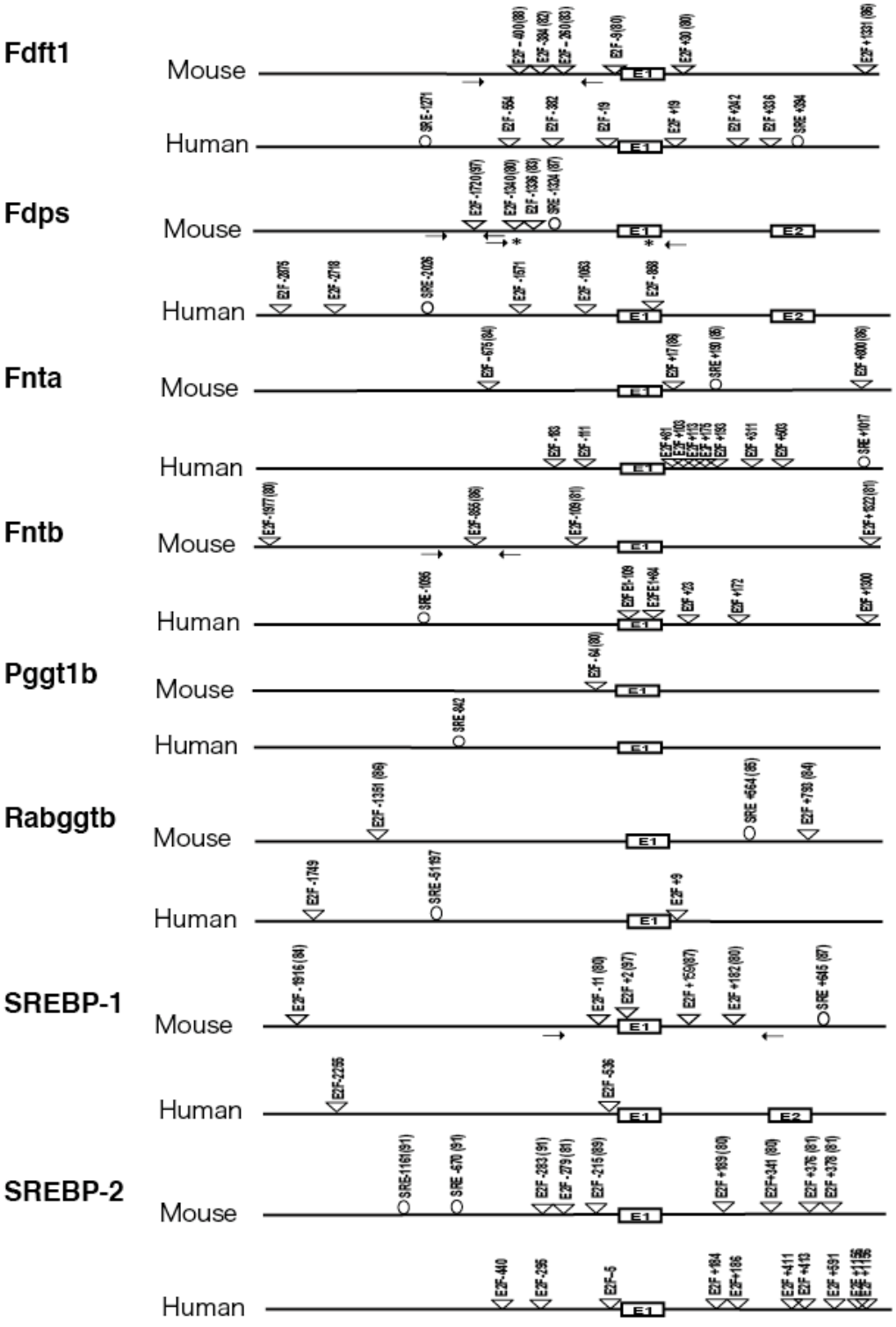
Fdft1
Mouse
Human
Fdps
Mouse
Human
Fnta
Mouse
Human
Fntb
Mouse
Human
Pggt1b
Mouse
Human
Rabggtb
Mouse
Human
SREBP-1
Mouse
Human
SREBP-2
Mouse
Human

Figure S11.

Figure S11. E2F- and SREBP-Binding Consensus Sequences on the Promoter of Genes Downregulated by pRb

Schematic presentation of promoter structure of the indicated genes on human and mouse genome. Positions of the DNA binding consensus sequence for E2Fs and SREBPs are indicated. Probability of each E2F binding consensus sequence in mouse genome is provided as score number in the parenthesis. The positions of ChIP primers used in Figure 6D and Figure S12 are indicated by arrows. The primers for *Fdps* promoter used in the lower panel of Figure 6D are indicated with asterisks (*). The sequence of these primers is listed in Table S4.

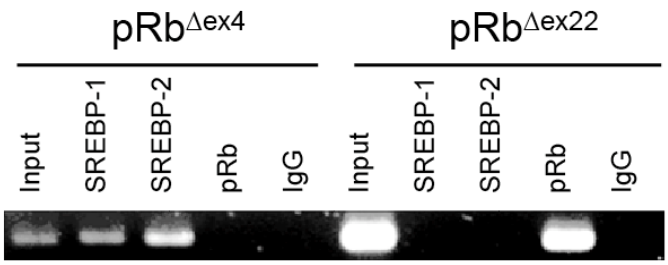

Figure S12. ChIP Assay of SREBPs and pRb Binding to the *Fdps* Promoter in AC61 Cells Infected with pRb Mutants

Binding of the indicated proteins to *Fdps* promoter in AC61 cells expressing the indicated pRb mutant was analyzed by ChIP assay. The positions of primers are shown in Figure S11 (*) and their sequence in Table S4 (*Fdps**).

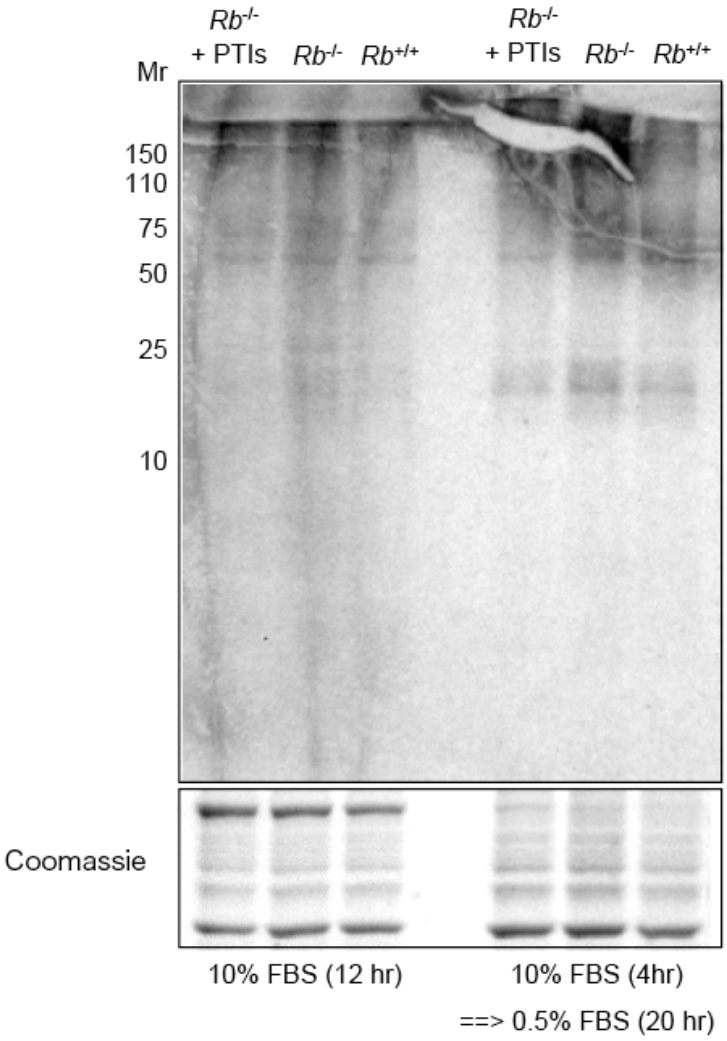

Figure S13. Global Visualization of Farnesylated Proteins in MEFs

MEFs with the indicated genotypes were treated under the indicated conditions and analyzed as in Figure 6F.

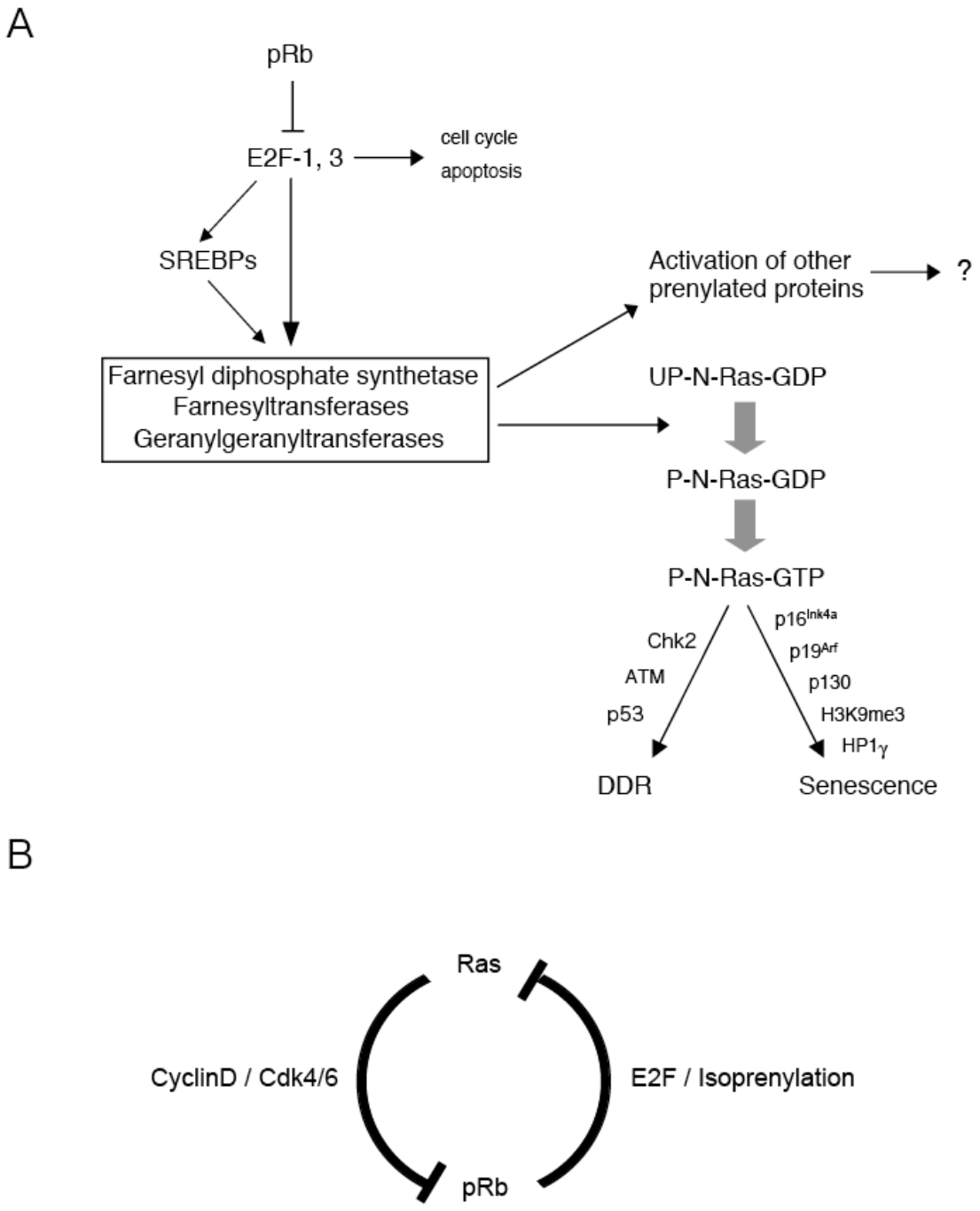

Figure S14. Current Model of the *Rb-N-ras* Genetic Interaction in Mouse C Cells and MEFs

(A) The signaling pathway which is generated by pRb and flows into Ras.

(B) Circuitry functional relationship between pRb and Ras.

Table S1. Twenty-Six Genes Downregulated by pRb with the Highest Confidence (Change p Value > 0.99998 Determined by Wilcoxon's Signed Rank Test) in Microarray Analysis Using Genechip Mouse 430.2 (Affymetrix)

Gene Description	Accesion Number	Functional Category
α4-tubulin	NM_009447.1	cell structure
Matrix metalloproteinase-3	NM_010809.1	proteolysis
Farnesyl diphosphate farnesyl transferase 1	BB028312	protein modification
EST	AK012577	
EST	AV148646	
EST	BB230894	
Squalene epoxidase	NM_009270	lipid synthesis
Grb14	NM_016719	signaling
Cdc6	NM_011799	cell cycle
EST	AV352204	
Glycine C-acetyltransferase	NM_013847	protein modification
Stearoyl-Coenzyme A desaturase 2	BB459479	lipid synthesis
EST	BM195254	
M8-9	BC014706	proton pump
EST	BQ175876	
Crabp1	NM_013496	nuclear receptor
Cytochrome p450	NM_020010.1	drug metabolism
Atp6v0b	NM_033617	proton pump
N-myc	M36277.1	transcription
Timm9	BF021416	mitochondrial receptor
Transferrin receptor	BB810450	iron transport
EST	BB727879	
Chondroitin sulfate proteoglycan 2	BM251152	ECM
EST	BC010217	
EST	AW554405	
Sphingosine kinase 2	BB550183	glycolipid metabolism

Table S2. Possible SREBP-Targeted Genes Found in 270 Genes Downregulated by pRb with Significantly High Confidence (Change p Value > 0.9998 Determined by Wilcoxon's Signed Rank Test) in Microarray Analysis Using Genechip Mouse 430.2 (Affymetrix)

Gene Description	Change p Value
Farnesyl diphosphate farnesyl transferase 1	>0.999980
Squalene epoxidase	>0.999980
Stearoyl-Coenzyme A desaturase 2	>0.999980
Sterol-C5-desaturase	>0.999973
Acetyl CoA transferase-like protein	>0.999970
NAD(P)-dependent steroid dehydrogenase-like protein	>0.999922
Mevalonate diphospho decarboxylase	>0.999899
Caveolin 2	>0.999833
Biotin acetyl-CoA-carboxylase	>0.999693
Hydroxysteroid (17-β) dehydrogenase 7	>0.999382
Isopentenyl-diphosphate delta isomerase	>0.999226
Fatty acid synthase	>0.998664

Table S3. RT-PCR Primer Sequences

Gene	Sense (5'→3')	Antisense (5'→3')
Fdft1	CCACCCGGAGGAGTTCTAT	AAGCTGCGACTGGTCTGATT
Fdps	CTGAGAAGGAGCTGGGACAC	TTCTACACACCAGCCCACTG
Fnta	AGCCGCAGGAAGAAGAGAT	TGATCTGGACCACTGGGTTAG
Fntb	AAGAGGCCTTCGACAACTGA	ACTATCTGGGGGATGGGTTC
Pggt1b	AGAAGGAGAACGGCTGGATT	TGTTCACCACATCCAAGGAG
Rabggt	CCACCTTCTGTACACGCTCA	TTCTCCCCAAATGTCTCCAG
SREBP-1	GATCAAAGAGGAGCCAGTGC	TAGATGGTGGCTGCTGAGTG
SREBP-2	GAGACCATGGAGACCCTCAC	GATAATGGGACCTGGCTGAA
GAPDH	ACCACAGTCCATGCCATCAC	TCCACCACCCTGTTGCTGT

Orientation and sequence of DNA primers used in RT-PCR of the indicated genes. Sequences were retrieved from GenBank (*Fdft1*, NM_010191; *Fdps*, NM_134469, *Fnta*, NM_008033; *Fntb*, NM_145927; *Pggt1b*, NM_172627; *Rabggt*, NM_011231; *SREBP-1*, NM_011480; *SREBP-2*, NM_033218 and *GAPDH*, NM_304088).

Table S4. ChIP Primer Sequences

Gene	Sense (5'→3')	Antisense (5'→3')
Fdft1	CCAGCCAACCCCTTAGGTAT	CGCTCCCACCTGTGTTTAG
Fdps	CCGGAGTGGTAGTGGTCTCT	GGGGTGAGGCAATAAGATCA
*Fdps**	GCTGGTTATTCCGGGATCTT	TTAGTGCCTCGGAGCTTCAC
Fntb	GTCTGTGGAGGCCAGAAAAG	AGCCCAGGAATGCAGAAGT
SREBP-1	TAGGCGAGCTGTCAGGATG	GGACCAGGCTTGAAGTTGAG

Orientation and sequence of DNA primers used in ChIP assays of the indicated genes in the upper panel of Figure 6D. *Fdps** represents the primer set used in the lower panel of Figure 6D and Figure S12. Their positions in mouse genome are indicated in Figure S11.